

Trichostatin A Enhances Vascular Repair by Injected Human Endothelial Progenitors through Increasing the Expression of TAL1-Dependent Genes

Carmen G. Pali¹, Branka Vulesevic^{2,3}, Sylvain Fraineau^{1,3}, Erinija Pranckeviciene^{1,3}, Alexander J. Griffith^{1,4}, Alphonse Chu¹, Hervé Faralli^{1,3}, Yuhua Li¹, Brian McNeill², Jie Sun¹, Theodore J. Perkins^{1,4,5}, F. Jeffrey Dilworth^{1,3}, Carol Perez-Iratxeta^{1,3}, Erik J. Suuronen^{2,3,6}, David S. Allan^{1,6} and Marjorie Brand^{1,3,6,*}

¹The Sprott Center for Stem Cell Research, Regenerative Medicine Program, Ottawa Hospital Research Institute, Ottawa, ON K1H8L6, Canada

²Division of Cardiac Surgery, University of Ottawa Heart Institute, Ottawa, ON K1Y4W7, Canada

³Department of Cellular and Molecular Medicine, University of Ottawa, Ottawa, ON K1H8L6, Canada

⁴Ottawa-Carleton Joint Program in Biomedical Engineering, University of Ottawa, Ottawa, ON K1H 8L6, Canada

⁵Department of Biochemistry, Microbiology and Immunology, University of Ottawa, Ottawa, ON K1H8L6, Canada

⁶Co-senior author

*Correspondence: mbrand@ohri.ca

<http://dx.doi.org/10.1016/j.stem.2014.03.003>

SUMMARY

A major goal of cell therapy for vascular diseases is to promote revascularization through the injection of endothelial stem/progenitor cells. The gene regulatory mechanisms that underlie endothelial progenitor-mediated vascular repair, however, remain elusive. Here, we identify the transcription factor TAL1/SCL as a key mediator of the vascular repair function of primary human endothelial colony-forming cells (ECFCs). Genome-wide analyses in ECFCs demonstrate that TAL1 activates a transcriptional program that promotes cell adhesion and migration. At the mechanistic level, we show that TAL1 upregulates the expression of migratory and adhesion genes through recruitment of the histone acetyltransferase p300. Based on these findings, we establish a strategy that enhances the revascularization efficiency of ECFCs after ischemia through *ex vivo* priming with the histone deacetylase inhibitor TSA. Thus, small molecule epigenetics drugs are effective tools for modifying the epigenome of stem/progenitor cells prior to transplantation as a means to enhance their therapeutic potential.

INTRODUCTION

Ischemic diseases occur when blood flow is interrupted or decreased and critical organs are deprived of oxygen. It has been well established that one of the most important factors in saving an organ after acute vascular injuries (such as acute limb ischemia, myocardial infarction, and stroke) is how quickly blood flow can be restored (Creager et al., 2012; Callum and Bradbury, 2000). Therefore, a major goal of cell therapy for vascular diseases is to increase the kinetics of blood flow recovery. Endothelial progenitors represent one of the most promising

cell-based strategies for increasing the rate of vascular repair after ischemic tissue damage (Leeper et al., 2010). Since the initial identification of cells with angiogenic properties in human peripheral blood (Asahara et al., 1997), diverse populations have been isolated under the common nomenclature “endothelial progenitor cells” (EPCs) and analyzed for their capacity to stimulate vascular repair following ischemic injuries (Fadini et al., 2012; Yoder, 2012). Overall, despite some uncertainty regarding the identity of various EPC populations, it has been well established that several sources of EPC-like cells are able to efficiently respond to ischemia by increasing capillary density, blood perfusion, and organ function. Furthermore, multiple studies have led to the view that different populations of EPCs improve vascular regeneration through different mechanisms, including (1) incorporation into injured endothelium followed by differentiation to form new blood vessels (e.g., Schwarz et al., 2012 and Ziebart et al., 2008) and/or (2) release of proangiogenic factors in the vicinity of the injured vessels to facilitate a coordinated repair process (e.g., Grunewald et al., 2006).

Endothelial colony-forming cells (ECFCs) (Ingram et al., 2004), also referred to as blood outgrowth endothelial cells (Lin et al., 2000), represent a homogeneous subpopulation of EPCs that can be isolated from human cord blood and peripheral blood. ECFCs possess unique properties that make them particularly attractive for cell-based regenerative therapy. First, ECFCs display robust clonal proliferative potential and express relatively high levels of telomerase (Ingram et al., 2004; Reinisch et al., 2009). In addition, they are able to differentiate into endothelial capillary-like tubes *in vitro* (Bouvard et al., 2010; Ingram et al., 2004; Reinisch et al., 2009) and form *de novo* functionally active human blood vessels *in vivo* (Au et al., 2008; Melero-Martin et al., 2007; Yoder et al., 2007). Most importantly, ECFCs have a demonstrated capacity to enhance revascularization when injected in animal models of ischemia (Bouvard et al., 2010; Saif et al., 2010; Schwarz et al., 2012). Whereas these studies have highlighted the potential of ECFCs for regeneration after ischemic injuries, we know very little about the molecular mechanism underlying the repair properties of these human progenitor cells that possess important clinical potential.

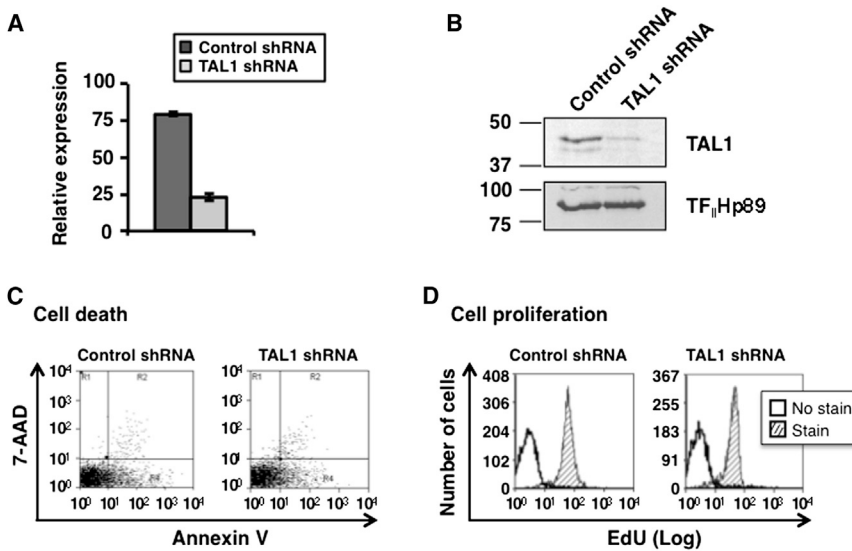


Figure 1. The Knockdown of TAL1 Does Not Affect ECFCs Survival and Proliferation

(A and B) TAL1 level is decreased in ECFCs after lentiviral delivery of anti-TAL1 shRNA relative to a control scrambled shRNA, as measured by qRT-PCR (A) and western blot (B).

(C) TAL1 KD does not induce necrosis or apoptosis as measured by fluorescence-activated cell sorting (FACS) after 7-AAD and annexin V staining, respectively.

(D) TAL1 KD has no effect on the proliferation of ECFCs as measured by FACS after EdU incorporation.

In (A), error bars represent SD of biological triplicates. In (B), molecular masses are in kDa. In (C) and (D), results have been reproduced multiple times ($n > 3$) with ECFCs obtained from different donors ($n > 2$). See also Figure S1.

Studies in mouse and zebrafish have established that transcription factors are primary determinants of vasculogenesis and angiogenesis during development (De Val and Black, 2009). In particular, the class II basic helix loop helix transcription factor TAL1 (also called SCL) is a critical regulator of the endothelial lineage. Indeed, TAL1 is required for specification of the hemogenic endothelium (Lancrin et al., 2009; Patterson et al., 2005) and for remodeling of the vasculature during development (Dooley et al., 2005; Shivdasani et al., 1995; Visvader et al., 1998). In addition, a recent study showed that, in the hemogenic endothelium, TAL1 acts as a determinant of endothelial cell fate through the inhibition of cardiomyogenesis (Van Handel et al., 2012). Postnatally, TAL1 is expressed in immature and newly formed blood vessels, including the tumor vasculature, whereas it is downregulated in quiescent endothelium (Chetty et al., 1997; Kallianpur et al., 1994). The significant contribution of TAL1 to developmental angiogenesis suggests that TAL1 could be important for the therapeutic function of injected ECFCs in the regeneration of blood vessels.

Here, we show that TAL1 is essential for mediating the vascular repair function of human ECFCs. Precisely, the role of TAL1 is to establish the transcriptional program that drives the migration of ECFCs by way of a mechanism that entails TAL1-mediated recruitment of the histone acetyltransferase p300 to specific effector genes. Finally, we show that treatment of ECFCs ex vivo with the histone deacetylase inhibitor TSA increases the expression of key genes within the TAL1 gene regulatory network and transplantation of these “primed” ECFCs increases the kinetics of blood flow recovery in mice with ischemic vascular injury.

RESULTS

TAL1 Is Necessary for Vascular Repair by Injected ECFCs

It is currently unknown whether TAL1 contributes to the therapeutic benefits of injected ECFCs to promote revascularization. To address this question, ECFCs were derived from human

umbilical cord blood using established protocols (Yoder et al., 2007). Phenotypic characterization confirmed that ECFCs display a typical, endothelial “cobblestone” morphology (Figure S1A available online) and express the early marker CD34 as well as a series of endothelial cell surface markers (CD31, CD105, CD144, vascular endothelial growth factor receptor 2, and von Willebrand factor), whereas they are devoid of the hematopoietic marker CD45 and the monocyte/macrophage marker CD14 (Figure S1B). To induce the knockdown (KD) of TAL1, ECFCs were infected with lentiviruses that express anti-TAL1 small hairpin RNA (shRNA) (or a scrambled shRNA as a control; Palić et al., 2011a, 2011b), resulting in a significant decrease of TAL1 levels (Figures 1A, 1B, and S2). We note that the KD of TAL1 does not affect the survival of ECFCs as measured by 7-amino-actinomycin D (7-AAD) and annexin V staining (Figure 1C) or their capacity to proliferate as measured by 5-ethynyl-2'-deoxyuridine (EdU) incorporation (Figure 1D). To determine whether the KD of TAL1 affects the ability of ECFCs to repair vascular injury, we used a mouse model of hindlimb ischemia. In this experiment, ischemia was induced by ligation of the left femoral artery, followed by ECFCs-mediated cell transplantation. Consistent with previous reports (Bouvard et al., 2010; Saif et al., 2010; Schwarz et al., 2012), injected ECFCs engraft into the ischemic muscle and display in vivo formation of blood vessels (Figures 2A and S1C). Furthermore, injected ECFCs increase arteriole density in the ischemic muscle (Figure 2B), which leads to a significantly improved blood perfusion recovery (Figure 2C). In contrast, ECFCs expressing reduced amounts of TAL1 do not engraft in the ischemic muscle and fail to improve blood flow recovery and arteriole density (Figure 2). Together, these results demonstrate that TAL1 is essential for the therapeutic revascularization function of injected ECFCs.

TAL1 Is Essential for the Migration and Adhesion Properties of ECFCs

To better understand the failure of ECFCs with TAL1 KD to promote revascularization in the ischemia animal model, we first

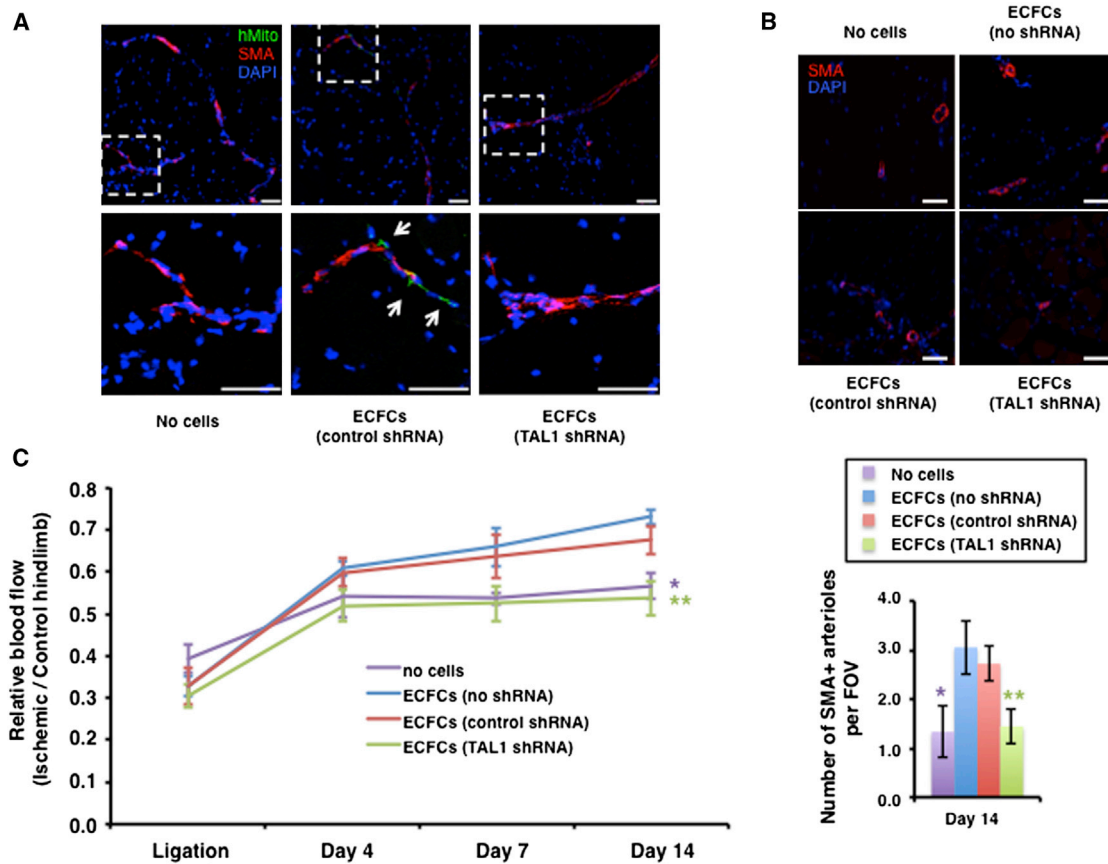


Figure 2. TAL1 Is Indispensable for the Vascular Repair Capacity of ECFCs

(A) Human ECFCs participate in the formation of blood vessels *in vivo* in a TAL1-dependent manner. Immunostaining was performed on ischemic muscles cryosections with a human-specific mitochondrial antibody (Ab) (hMito, green) and a smooth muscle actin Ab (SMA, red) 14 days after injection of PBS (no cells), ECFCs (control shRNA), or ECFCs with a KD of TAL1 (TAL1 shRNA). Nuclei were stained with DAPI (blue). Arrows indicate human cells. The scale bar represents 50 μ m. (B) ECFCs with a KD of TAL1 fail to increase arteriole density in the ischemic muscle. Top panel, representative images of arterioles (SMA⁺, red) and nuclei (DAPI, blue) at day 14 in the ischemic muscle. The scale bar represents 50 μ m. Bottom panel, quantification of SMA⁺ vessels. FOV, field of view. (C) ECFCs with a KD of TAL1 fail to improve blood perfusion recovery in a mouse model of hindlimb ischemia. Relative blood flow (ischemic/nonischemic hindlimb) was measured by laser Doppler perfusion imaging immediately after induction of hindlimb ischemia (ligation) and at the indicated time points after intramuscular injection of PBS (no cells), unmodified ECFCs (no shRNA), or ECFCs infected with a lentivirus expressing either an anti-TAL1 shRNA (TAL1 shRNA) or a scrambled shRNA (control shRNA).

In (B) and (C), results are expressed as the mean \pm SEM (six mice per group, two independent cord blood donors for each group). * $p < 0.05$; ** $p < 0.01$.

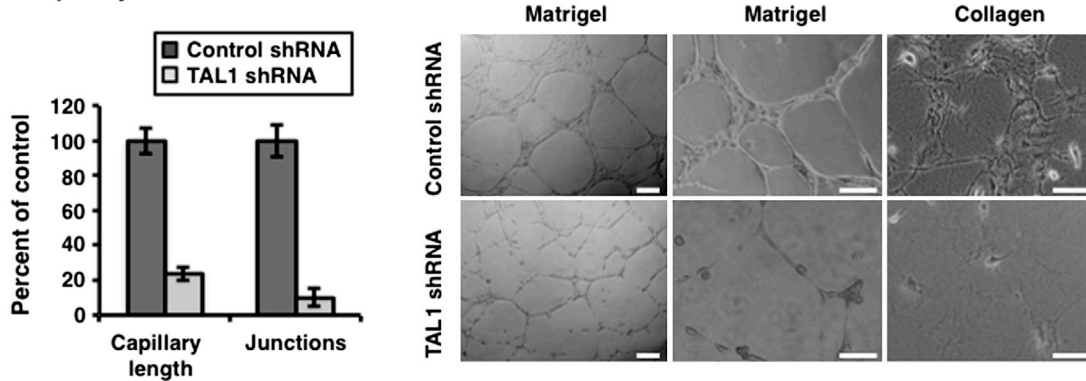
examined the capacity of these cells to form a vascular network upon differentiation on extracellular Matrigel and collagen matrices. We found that ECFCs with reduced levels of TAL1 are unable to form complete, fully connected capillary-like structures (Figure 3A), demonstrating that TAL1 is essential for *in vitro* angiogenesis of ECFCs.

To identify the step(s) of vessel morphogenesis that are regulated by TAL1, we sought to examine the consequences of TAL1 KD on ECFC adhesion, migration, and chemotaxis. First, we tested the adhesion property of ECFCs and found that adhesion is severely compromised by the KD of TAL1 (Figure 3D). Then, a radius cell migration assay was used to measure the kinetics of ECFC migration toward a central “cell-free” zone. This experiment revealed a major defect in the migration of TAL1 KD cells with virtually no cells invading the central area, in contrast to control ECFCs, which completely fill the central gap within 30 hr (Figure 3B). As migration toward the chemokine stromal-cell-

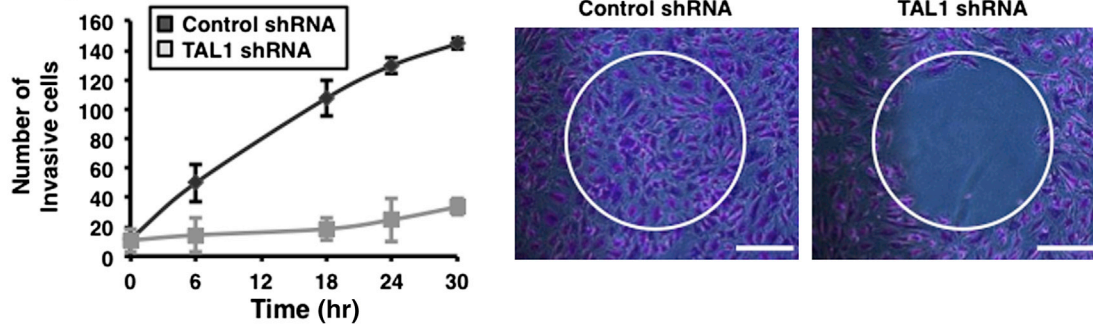
derived factor 1 (SDF-1) is essential for the recruitment of endothelial progenitors to sites of ischemic injury (Ceradini et al., 2004), we also tested the migration of ECFCs by chemotaxis toward SDF-1 in a modified Boyden chamber assay. Upon TAL1 KD, we observed a marked reduction in the migration of ECFCs toward SDF-1 (Figure 3C). SDF-1 regulates cell motility through binding to the CXC chemokine receptor 4 (CXCR4) that is present at the surface of endothelial cells. Therefore, we measured the levels of CXCR4 in TAL1 KD ECFCs. We found that ECFCs with a KD of TAL1 express reduced levels of CXCR4 both *ex vivo* prior to transplantation (Figure 3E) and *in vivo* after transplantation in the ischemic muscle (Figure 3F). These results show that the SDF-1/CXCR4 axis is intact in ECFCs and is altered upon TAL1 KD.

In summary, results from the phenotypic analyses upon TAL1 KD establish TAL1 as a major mediator of ECFCs-mediated blood vessel morphogenesis.

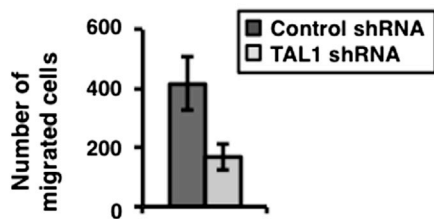
A Capillary-like structure formation



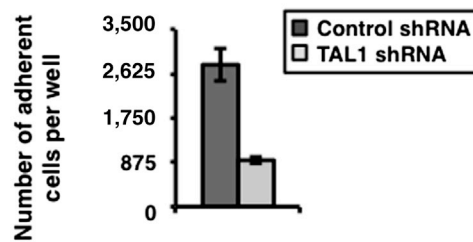
B Migration



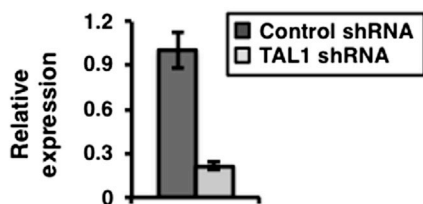
C Chemotaxis (SDF-1)



D Adhesion



E hCXCR4 expression - ex vivo (prior to transplantation)



F hCXCR4 expression - in vivo (4 days posttransplantation)

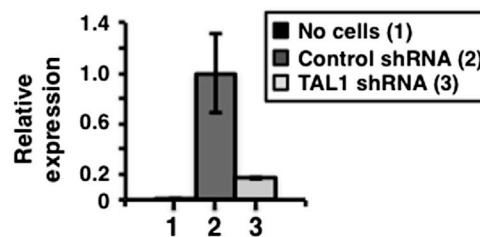


Figure 3. TAL1 Is Indispensable for Adhesion, Migration, and Chemotaxis of ECFCs

(A) TAL1 KD leads to a profound defect in capillary-like structure formation after ECFCs plating on Matrigel and collagen. Left panel, quantification of the average length of capillary-like structures and the number of junctions, respectively, by automatic counting with the AngioQuant software. Right panel, representative images (bright field). The scale bar represents 50 μm for the left-most row and 20 μm for the middle and right rows.

(B) TAL1 KD inhibits ECFCs migration as measured by gap closure assay. Left panel, number of ECFCs that have invaded a defined “cell-free” zone (inside of white circle on the right panel) at the indicated time points ($n = 3$). Right panel, cells at the 30 hr time point that were fixed and stained. The scale bar represents 20 μm .

(legend continued on next page)

Genome-wide Mapping of TAL1 Target Genes in ECFCs

To gain further insight into the molecular mechanism through which TAL1 promotes adhesion and migration, we set out to identify TAL1 target genes in ECFCs. Genome-wide occupancy of TAL1 in ECFCs was investigated by chromatin immunoprecipitation coupled to massively parallel DNA sequencing (ChIP-seq). As a negative control, ChIP-seq was performed using normal immunoglobulin G (IgG). This experiment led to the identification of 1,679 TAL1-binding sites genome-wide ($p < 10^{-5}$; Figure 4). An analysis based on the rate of conversion of background to foreground signal (Fong et al., 2012; Palii et al., 2011b) indicates that sequencing depth was sufficient for genome-wide coverage (data not shown). Validating the quality of ChIP-seq data, TAL1 binding was confirmed by independent ChIP-quantitative PCR (qPCR) on all tested sites (Figures 5A and S3A). Importantly, a decrease in ChIP signal is observed upon TAL1 KD, which validates the specificity of TAL1 ChIP (Figures 5A and S3A).

To identify DNA sequences that are statistically overrepresented under the peaks of TAL1 binding, we used a de novo motif search algorithm (Fong et al., 2012; Palii et al., 2011b). Enriched DNA motifs include E-boxes (i.e., TAL1-binding site), as well as binding sites for GATA, ETS, and FOX families of transcription factors (Figure 4A; see Figure S4A for a complete list of motifs). Furthermore, a search for preferred distances between DNA sequences led to the identification of composite motifs that are overrepresented under the peaks of TAL1 binding, including an E-box_GATA motif and an ETS_E-box motif (Figures 4B and S4B).

Assigning ChIP-seq peaks to gene regulatory elements (GREs) revealed that TAL1 occupies mostly intronic (32%) and intergenic (36%) regions of the genome (Figure 4C). Importantly, some of these distal sites have been validated previously in transgenic mouse embryos as being functional endothelial enhancers such as the intronic enhancer of the *Gata2* gene (Khandekar et al., 2007). In addition to distal GREs, TAL1 binds to proximal promoters (Figure 4C) with the region around the transcription start site (TSS) containing the highest density of TAL1 peaks (Figure 4D). Examples of genes with proximal promoter binding of TAL1 include both known (*CDH5*; Deleuze et al., 2007) and, to our knowledge, novel (*EPHB4*; Figure 4E) endothelial targets.

To gain insight into the overall function of TAL1 target genes in ECFCs, we performed a global search for overrepresented functional categories using the Genomic Regions Enrichment of Annotation Tool (GREAT) v.2.02 (McLean et al., 2010). This analysis revealed that TAL1 target genes are highly enriched within functional categories related to the formation of blood vessels such as “blood vessel development” ($p = 1.37 \times 10^{-21}$), “blood vessel morphogenesis” ($p = 5.64 \times 10^{-20}$), and “angiogenesis” ($p = 6.98 \times 10^{-18}$; Figure 4F; Table S1). Furthermore, TAL1 target

genes are enriched within regulatory pathways that are critical to the vascular system including platelet-derived-growth-factor- and vascular endothelial growth factor (VEGF)-signaling pathways (Figure 4G; Table S1). For example, TAL1 binds to an active endothelial enhancer upstream of the gene coding for the proangiogenic growth factor VEGFA (Figure S6A). Finally, enriched categories from the Mouse Genome Informatics (MGI) expression database indicate that TAL1 target genes are expressed in the arterial system, dorsal aorta, and decidua (Figure 4H; Table S1). Overall, this global analysis indicates that, in ECFCs, TAL1 binds to genes that are involved in the formation of blood vessels, a result that is highly consistent with our finding that TAL1 is essential for postnatal revascularization by injected ECFCs (Figure 2).

To identify, among TAL1 target genes, those that are functionally dependent on TAL1 for their expression, we profiled gene-expression changes occurring upon TAL1 KD in ECFCs (using Affymetrix microarray on three independent ECFCs clones generated from three distinct cord blood donors; see Table S1) and intersected the list of statistically significant changing genes with the list of TAL1 targets (Table S1). Validating this experiment, *CDH5*, a previously known TAL1-activated gene (Deleuze et al., 2007), which codes for the adherens junction molecule vascular endothelial-cadherin was identified and confirmed by ChIP-qPCR and quantitative RT-PCR (qRT-PCR) (Figure 5A). In addition, our analysis revealed multiple TAL1-activated genes that are involved in promoting endothelial cell migration and adhesion. For example, TAL1 activates the gene coding for the ephrin-B2 ligand (*EFNB2*; Table S1; Figure 5A), a transmembrane tyrosine kinase that mediates cell-cell contact through its interaction with EphB receptors (mostly EphB4). Ephrin-B2 plays a critical role in angiogenesis and vasculogenesis (Salvucci and Tosato, 2012). Interestingly, the *EPHB4* gene, which codes for ephrin-B2 receptor, is also targeted by TAL1 (Figure 4E), but its expression does not change upon TAL1 KD in ECFCs (data not shown), highlighting the importance of performing gene-expression profiling in addition to ChIP-seq. In addition to *CDH5* and *EFNB2*, multiple other genes that are known to play important roles in cell migration and adhesion were identified as TAL1 targets (Figure S3B; Table S1). Thus, TAL1 activates multiple “effector” genes that directly impact the function of endothelial progenitors by promoting cell migration and adhesion. Besides effector genes, our results show that TAL1 also activates genes encoding transcription factors that are themselves essential for endothelial cell function. Notably, we identified the genes coding for SOX7 (Costa et al., 2012) and HOXA9 (Bruhl et al., 2004) as being directly bound to and activated by TAL1 (Figure 5A).

Taken together, these data suggest that TAL1 promotes migration and adhesion of ECFCs both directly through the

(C) TAL1 KD decreases ECFCs migration by chemotaxis toward SDF-1 as measured in a modified Boyden chamber migration assay ($n = 3$).

(D) TAL1 KD decreases ECFCs adhesion on plate ($n = 3$).

(E) Reduction of CXCR4 levels in TAL1 KD ECFCs prior to transplantation. qRT-PCR was performed on RNA isolated from ECFCs with normal (control shRNA) or reduced (TAL1 shRNA) levels of TAL1 using primers specific for human CXCR4 (hCXCR4). qRT-PCR values are expressed relative to human GAPDH ($n = 3$).

(F) Reduction of human CXCR4 levels in murine ischemic muscles transplanted with TAL1 KD ECFCs. qRT-PCR was performed on RNA isolated from ischemic muscle from mice previously injected with PBS (no cells), ECFCs (control shRNA), or TAL1 KD ECFCs (TAL1 shRNA). qRT-PCR values for hCXCR4 are expressed relative to rodent GAPDH \pm SEM ($n = 3$ mice per group).

In (A)–(E), error bars represent SD of biological triplicates. See also Figure S2.

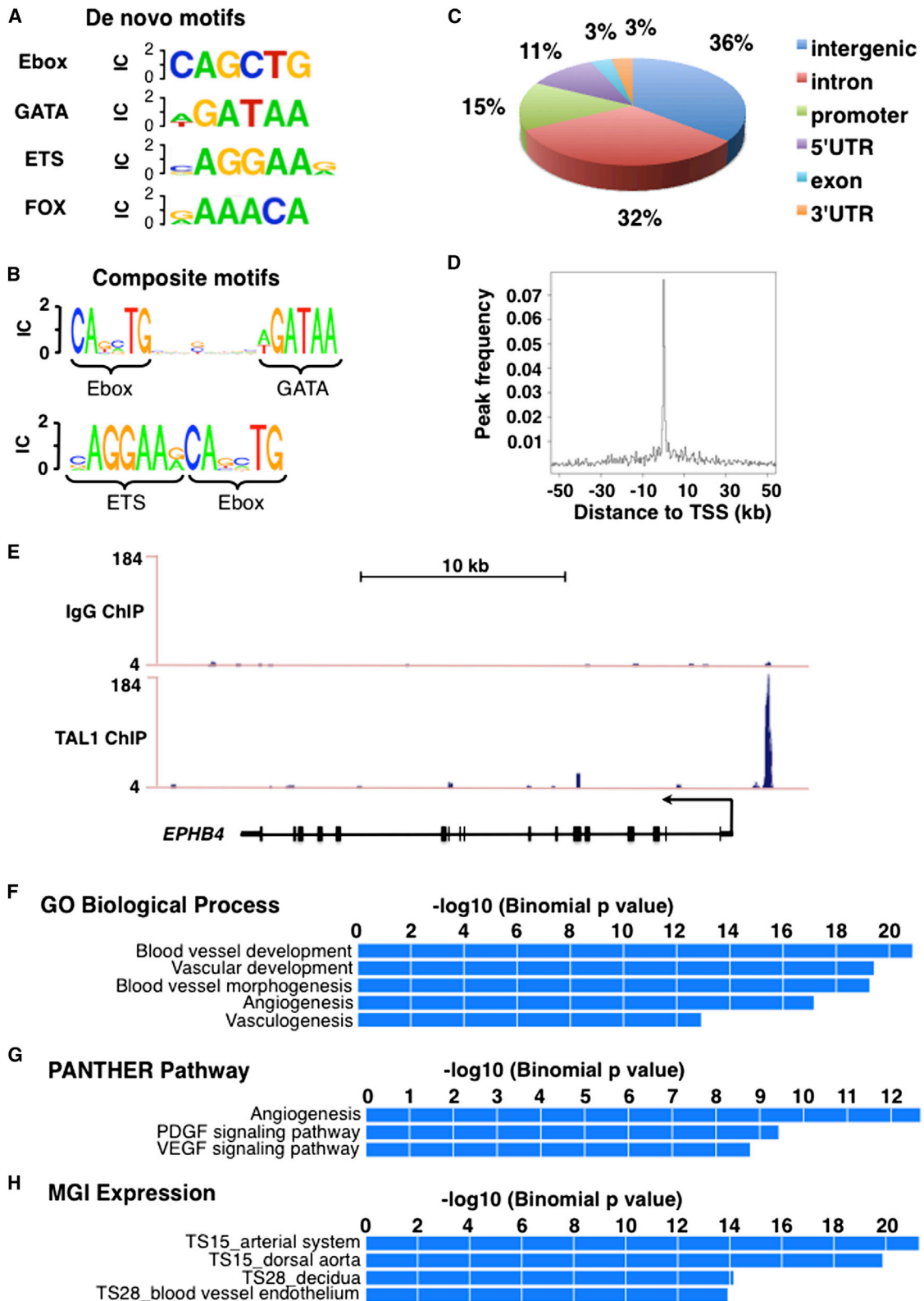


Figure 4. ChIP-Seq Analysis of TAL1 Genomic Binding in ECFCs

(A) Top four DNA motifs overrepresented under the peaks of TAL1 binding as identified by de novo motif discovery.

(B) Composite motifs overrepresented under the peaks of TAL1 binding.

(C) Genomic distribution of TAL1-binding sites.

(legend continued on next page)

activation of critical effector genes (e.g., *EFNB2* and *CDH5*) and indirectly through the activation of transcription factors that in turn modulate endothelial cell function (e.g., *SOX7* and *HOXA9*). Thus, our results provide a molecular mechanism to explain the phenotypic effects (decrease in migration and adhesion) observed upon TAL1 KD in ECFCs.

TAL1 Recruits the Histone Acetyltransferase p300 to Activate Gene Expression

Next, we sought to determine the mechanism through which TAL1 activates gene expression in ECFCs. Because TAL1 interacts with the histone acetyltransferase (HAT) p300 in erythroid cells (Huang et al., 1999), we hypothesized that TAL1 could activate transcription through the recruitment of this coactivator. Consistent with this, ChIP experiments demonstrate that p300 is bound to TAL1-activated genes *CDH5*, *EFNB2*, *SOX7*, and *HOXA9* in ECFCs (Figure 5B). Furthermore, the KD of p300 decreases the expression of these genes (Figure 5C) and leads to important defects in the capacity of ECFCs to migrate and to form a vascular network (Figures S5A and S5B), similar to the phenotypic effects observed upon TAL1 KD. Importantly, p300 binding is lost on TAL1 target genes upon TAL1 KD (Figure 5B), which confirms the dependence on TAL1 for p300 recruitment. Finally, the loss of p300 binding upon TAL1 KD is accompanied by a decrease in histone H3 acetylation (Figure 5D) and gene transcription (Figure 5A). Taken together, these results demonstrate that, in ECFCs, TAL1 activates gene expression through the recruitment of p300 that leads to increased histone acetylation (Figure 6G, left panel).

The Histone Deacetylase Inhibitor TSA Enhances the Migratory Capacity of ECFCs through a TAL1-Dependent Mechanism

Genome-wide studies have shown that active genes regulated by HATs are also targeted by histone deacetylases (HDACs) that serve to temper histone acetylation levels (Wang et al., 2009). This suggests that HDAC inhibitors could increase gene transcription by displacing the balance toward a higher level of histone acetylation. To test this possibility, we first examined whether *ex vivo* treatment of ECFCs with the HDAC inhibitor TSA increases the expression of TAL1-dependent genes. We found that incubation of ECFCs with TSA leads to a 2- to 3-fold increase in histone H3 acetylation level (Figure 6A) and in the expression level (Figure 6B) of TAL1-dependent genes. Furthermore, TSA treatment leads to an increased binding of the bromodomain-containing histone acetyltransferase p300 (Zeng and Zhou, 2002) at TAL1 target genes (Figure 6D). These results are consistent with a model in which TSA treatment increases gene transcription by displacing the balance toward a higher level of histone acetylation (Figure 6G).

Next, we wanted to determine whether TSA treatment could also affect the TAL1 protein. First, we examined TAL1 subcellular localization and found no change in TAL1 nuclear staining upon TSA treatment (Figure S5C). Second, we explored whether TSA treatment could modify the acetylation status of TAL1. Consistent with a previous study (Huang et al., 2000), we detected strong acetylation of TAL1 in the murine erythroleukemia (MEL) cell line (Figure S5D, right panel). In contrast, we could not detect acetylated TAL1 in ECFCs under the same conditions (Figure S5D, left panel). Most importantly, TAL1 acetylation status is not changed upon TSA treatment of either MEL cells or ECFCs (Figure S5D). Finally, we examined whether TSA treatment would alter TAL1 genomic binding in ECFCs. We repeated TAL1 ChIP-seq experiments in TSA-treated versus nontreated ECFCs and compared TAL1 genome-wide binding between the two conditions. We found a very high correlation for TAL1 binding in TSA-treated versus nontreated ECFCs with a Pearson correlation coefficient of 0.96 (Figure 6E, left panel). To assess the significance of this result, we performed multiple comparisons of published TAL1 ChIP-seq data sets. This analysis indicated that TAL1 binding in TSA-treated and nontreated ECFCs displays a level of similarity as good as or better than TAL1 binding between ChIP-seq replicates (Figure S5E). Furthermore, the ChIP-seq enrichment profiles show no change in TAL1 binding on a large portion of chromosome 6 (Figure 6E, right) and on the *VEGFA* locus (Figure S6A). Therefore, TAL1 genomic binding is not altered upon TSA treatment of ECFCs. Altogether, these results support the model depicted in Figure 6G where TSA treatment of ECFCs acts mostly through increasing histone acetylation and gene expression rather than modifying TAL1 binding to the genome.

As TAL1 activates genes involved in migration, we reasoned that treatment of ECFCs with TSA could improve the migratory capacity of ECFCs. Consistent with this hypothesis, we found that TSA treatment, whereas not affecting the morphology of ECFCs (Figure 7A), leads to a striking increase in the migration kinetics of these cells (Figure 6F). Importantly, this effect is dependent on TAL1 as the migration of TSA-treated ECFCs is abolished upon TAL1 KD (Figure 6F). Taken together, these results demonstrate that TSA treatment increases the migratory capacity of ECFCs through a TAL1-mediated mechanism.

TSA Treatment Enhances ECFCs Revascularization Efficiency

In the clinical setting, it has been shown that one of the most important factors in saving an organ after acute ischemia is how quickly blood flow can be restored (Creager et al., 2012; Callum and Bradbury, 2000). Thus, our finding that TSA increases the kinetics of ECFC migration (Figure 6F) suggests that this treatment might have an important clinical impact by increasing the speed at which blood flow can be restored after

(D) Frequency of TAL1 peak location relative to the closest TSS.

(E) TAL1 binds to the *EPHB4* gene proximal promoter. TAL1 and negative control (IgG) ChIP-seq density plots were generated from raw data and loaded into the University of California, Santa Cruz genome browser. The *EPHB4* gene is depicted at the bottom.

(F) Gene Ontology (GO) biological process analysis for TAL1 target genes (top five categories).

(G) PANTHER pathway analysis for TAL1 target genes (top three pathways).

(H) Expression of TAL1 target genes in the MGI database (top four categories).

For a full list of motifs (A and B), see Figure S4. For a full list of enriched categories (F–H), see Table S1. See also Figures S3 and S4.

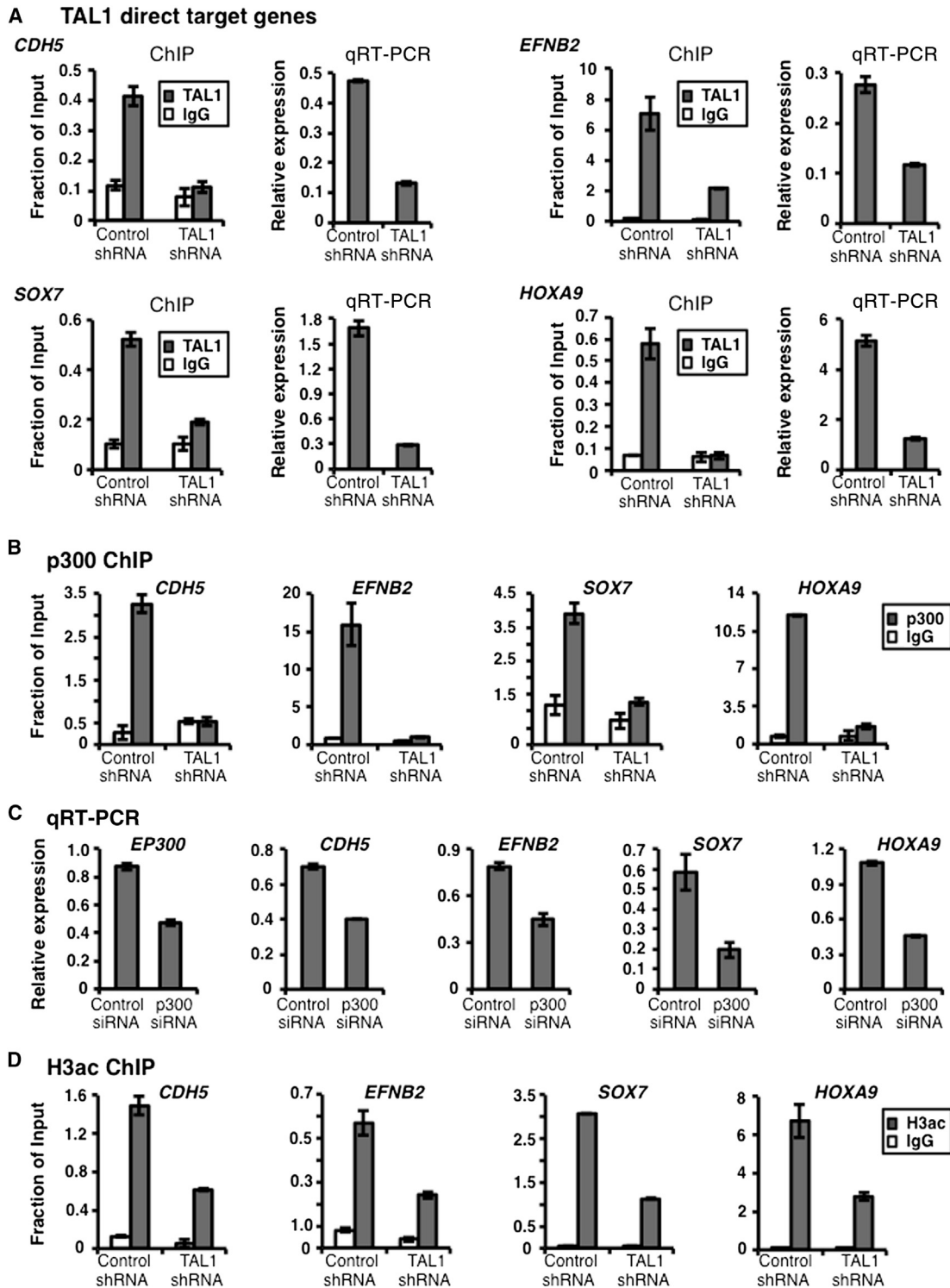


Figure 5. TAL1 Activates Gene Expression through Recruitment of the Acetyltransferase p300 and Increase in Histone H3 Acetylation

(A) Validation of TAL1-activated genes in ECFCs.

(B) p300 is recruited to TAL1 target genes in a TAL1-dependent manner.

(C) The KD of p300 leads to a decrease in the expression of TAL1 target genes. siRNA, small interfering RNA.

(D) The KD of TAL1 leads to a decrease in histone H3 acetylation on its target genes.

(legend continued on next page)

ischemic injury. To test this hypothesis, ECFCs were pretreated with TSA ex vivo prior to transplantation into ischemic mouse muscle. We found that TSA treatment leads to a dramatic increase in the rate of blood flow recovery because mice injected with TSA-treated ECFCs attain 90% of maximal blood flow recovery as early as 4 days after cell therapy compared to 10 days for mice injected with non-TSA-treated cells (Figures 7B and 7C). Therefore, ex vivo treatment with TSA significantly improves the kinetics of ECFC-mediated vascular repair in vivo. Importantly, the effect of TSA on ECFCs is mediated at least in part through TAL1 target genes as decreases in migration and blood flow recovery are also observed upon knockdown of the TAL1 target gene *CDH5* in TSA-treated cells (Figures S6D–S6H).

To obtain additional insight into the mechanism through which ex vivo treatment with TSA improves the in vivo function of transplanted ECFCs, we measured arteriole density in the ischemic muscle. We found that, 4 days after injection, arteriole density is increased by 60% in mice transplanted with TSA-treated ECFCs (Figure 7D), which is highly consistent with the increased kinetics of blood flow recovery (Figures 7B and 7C). Furthermore, we observed less necrosis in the ischemic muscle of mice injected with TSA-treated ECFCs compared to mice injected with unmodified ECFCs (data not shown). Taken together, these results confirm that in vivo revascularization is more efficient with TSA-treated ECFCs. Interestingly, we also detect a strong increase in the expression of human CXCR4 in vivo in the ischemic muscle of mice transplanted with TSA-treated ECFCs (Figure 7F), suggesting that TSA treatment increases the SDF-1/CXCR4 axis that is essential for migration of ECFCs. However, we do not observe a higher percentage of vessels containing human ECFCs in mice injected with TSA-treated ECFCs, even though both TSA-treated and nontreated cells engraft in the ischemic muscle after 4 days (Figure 7E). Finally, we detect a strong increase in the level of human VEGFA (a TAL1-target gene; Figures S6A–S6C) in vivo in the ischemic muscle of mice transplanted with TSA-treated ECFCs (Figure 7G), suggesting that TSA can also improve the paracrine function of ECFCs. Taken together, these results suggest that ex vivo treatment with TSA improves the revascularization potential of ECFCs both by promoting migration via increased CXCR4 expression and through paracrine effects via increased expression of VEGFA that can act both on ECFCs and on resident murine endothelial cells.

DISCUSSION

Revascularization by injected ECFCs is a promising strategy to enhance vascular repair in ischemic diseases (Bouvard et al., 2010; Moubarik et al., 2011; Saif et al., 2010; Schwarz et al., 2012). Despite significant advances in our understanding of ECFCs, the gene-regulatory mechanisms that control the function of these therapeutically important cells remain elusive. Focusing on the transcription factor TAL1, we present here an in-depth characterization of human primary ECFCs in the

context of their role as a potential therapeutic cell source for regenerative therapy. First, we demonstrate that TAL1 is necessary for the postnatal revascularization function of human ECFCs in vivo. Interestingly, we found that TAL1 is required for the migration and adhesion of ECFCs, but not for their proliferation. Mechanistically, resolution of the genome-wide TAL1 regulatory network demonstrates that this effect is mediated by the ability of TAL1 to directly activate multiple adhesion and migration effector genes through epigenetic mechanisms that entail recruitment of the acetyltransferase p300 and subsequent histone H3 acetylation. Finally, using the HDAC inhibitor TSA, we are able to further increase histone acetylation levels, leading to increased expression of TAL1 target genes, which in turn significantly improves the vascular repair function of ECFCs. Thus, our study provides proof of principle that HDAC inhibitors can be used to ameliorate the therapeutic function of ECFCs.

Studies at the Gene Level Are Effective in Optimizing the Design of New and Improved Therapies Using Stem/Progenitor Cells

Characterization of the TAL1 transcriptional network in ECFCs allowed us to identify a major role for this factor in the activation of genes that are essential mediators of endothelial cell function. Furthermore, we showed that TAL1 activates these genes through recruitment of the HAT p300. This mechanistic insight served as the basis for examining the HDAC inhibitor TSA as a potential epigenetic drug to augment the vascular repair function of ECFCs in vivo. Thus, the mechanistic study of TAL1 was a prerequisite for designing a strategy to improve the therapeutic function of ECFCs. In addition, molecular studies allowed us to measure the effect of TSA directly on the acetylation and expression status of TAL1-dependent genes, which was essential to precisely adjust the dose of TSA and avoid potentially adverse effects such as inhibition of endothelial differentiation that is observed when TSA is used at higher concentrations (Rössig et al., 2005; C.G.P., S.F., and M.B., unpublished data). This illustrates how mechanistic insights into gene-regulatory mechanisms may be exploited to develop improved therapeutic strategies using stem/progenitor cells.

Improving ECFC Therapeutic Potential through Epigenetic Drugs

Here, we have shown that stimulating ECFCs by pretreatment with the HDAC inhibitor TSA enhances their therapeutic potential. Specifically, ex vivo treatment of ECFCs with TSA markedly increases the rate of blood flow recovery, a highly desirable goal in the context of acute ischemic diseases where the rapidity of restoring oxygen supply to hypoxic tissues is critical for patient recovery (Creager et al., 2012). To our knowledge, this is the first study demonstrating that ex vivo priming with an epigenetic drug prior to transplantation can dramatically improve the revascularization efficiency of ECFCs. Furthermore, this approach has many advantages. First, administering the drug to the cells, as opposed to the patient, limits potentially adverse secondary

For (A), (B), and (D), ChIP-qPCR and qRT-PCR were performed in the presence of normal (control shRNA) or reduced (TAL1 shRNA) levels of TAL1 using a TAL1 Ab or IgG as a negative control. For (C), qRT-PCR was performed in the presence of normal (control siRNA) or reduced (p300 siRNA) levels of p300. ChIP-qPCR values are expressed as a fraction of input with error bars corresponding to SD. qRT-PCR values are expressed relative to the internal control *GAPDH* with error bars corresponding to SD. For a full list of TAL1 target genes, see Table S1.

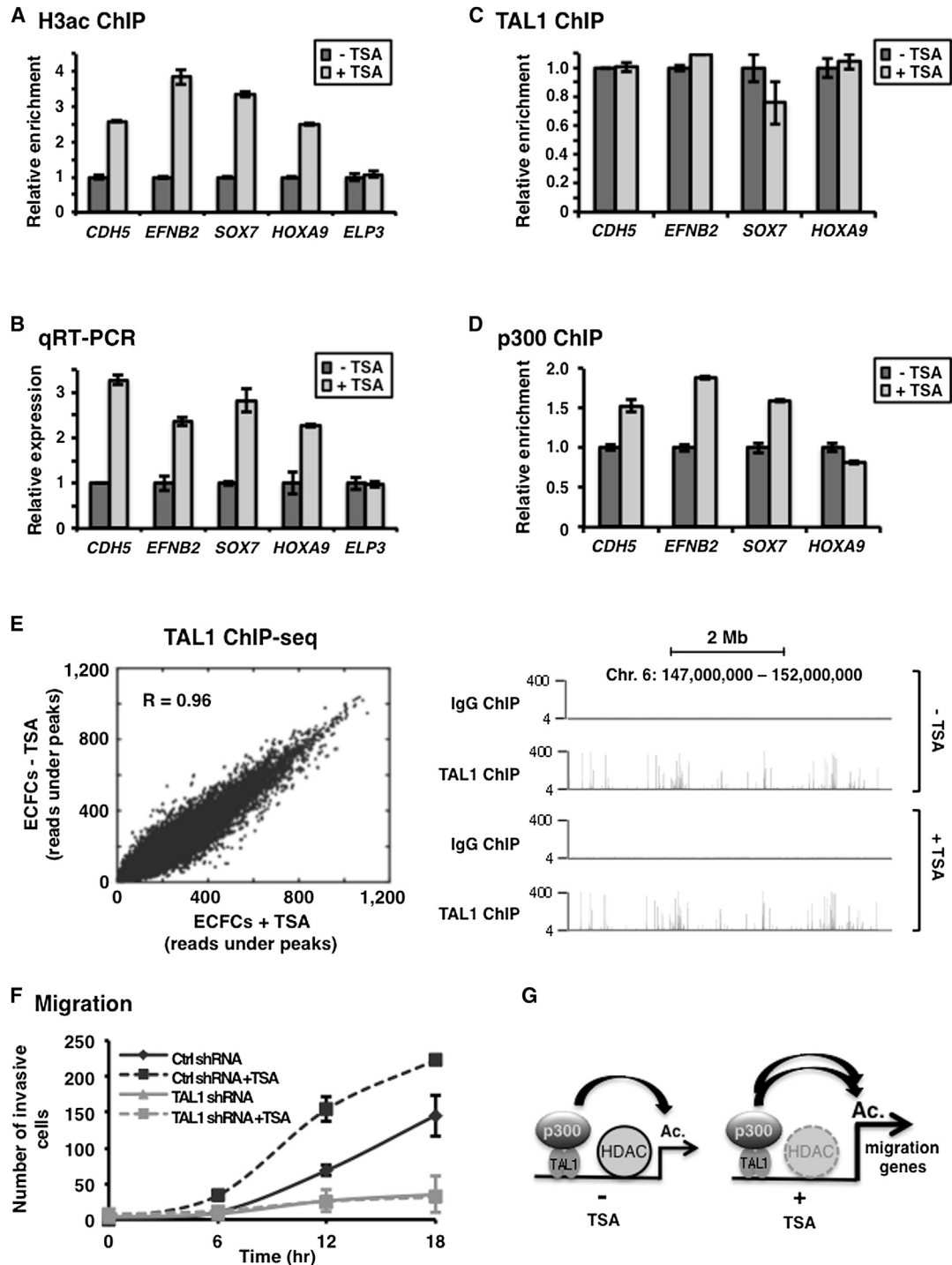


Figure 6. TSA Treatment Increases the Expression of TAL1 Target Genes and Augments the Migratory Capacity of ECFCs

(A and B) TSA treatment increases histone H3 acetylation (A) and expression (B) of TAL1 target genes.

(C) TSA treatment does not change TAL1 binding to its target genes.

(D) TSA treatment stabilizes p300 binding to TAL1 target genes.

(E) TSA treatment does not alter TAL1 binding genome wide. Left panel, correlation plot of TAL1 genomic binding in TSA-treated (x axis) versus untreated (y axis) ECFCs as measured by ChIP-seq. The Pearson's linear correlation coefficient (R value) is indicated (also see Figure S5E). Right panel, representative example of TAL1 binding to a 6 Mb region on chromosome 6. IgG ChIP-seq served as a negative control.

(F) Pretreatment with TSA increases the migration kinetics of ECFCs in a TAL1-dependent manner. Migration of ECFCs containing normal (Ctrl shRNA) or reduced (TAL1 shRNA) levels of TAL1 and pretreated with TSA (+TSA) or not (-TSA) was measured by counting the number of cells that have invaded a central cell-free zone at the indicated time points (n = 3). Error bars correspond to SD.

(legend continued on next page)

effects from a drug administered systemically. Second, the accessibility of ex-vivo-cultured ECFCs facilitates the optimization of drug dosage to achieve maximal therapeutic benefit. Finally, in contrast to gene therapy approaches that work through modifying the genome to ameliorate stem cell function, changes in gene expression triggered by epigenetic drugs are transient and as such less likely to have long-term, potentially harmful consequences to the patient. This is particularly relevant for endothelial progenitors as uncontrolled vascularization can facilitate tumor growth and metastasis (Liu et al., 2012). Thus, ex vivo treatment with HDAC inhibitors may provide an efficient approach to augment the therapeutic potential of human ECFCs.

The TAL1 Gene-Regulatory Network in ECFCs

Resolution of the TAL1 transcriptional network by ChIP-seq and gene-expression profiling suggests that TAL1 is part of a larger network of transcription factors that regulate ECFCs. First, TAL1 directly binds to and activates the genes coding for transcription factors SOX7 and HOXA9, both of which are essential regulators of endothelial cells (Bruhl et al., 2004; Costa et al., 2012). Furthermore, analysis of the DNA sequence under TAL1 peaks identified several motifs that are recognized by transcription factors of the GATA, ETS, and FOX families, suggesting that TAL1 could cooperate with these factors to regulate gene expression. Interestingly, comparing the DNA sequences over-represented under TAL1 peaks in ECFCs versus cells of the hematopoietic lineage, we note that some motifs are reminiscent of TAL1 binding in hematopoiesis (i.e., E-box_GATA [Fujiwara et al., 2009; Pali et al., 2011b; Soler et al., 2010; Wilson et al., 2010] and ETS_E-box [Pali et al., 2011b]), whereas others appear specific to ECFCs such as a FOX motif (Figure 4A). This suggests that TAL1 cooperates with distinct factors in ECFCs versus hematopoietic cells. Taken together, these data emphasize that TAL1 is part of a larger transcriptional regulatory network that comprises many other factors with which it interacts to regulate gene expression in ECFCs.

Whereas we have shown that TAL1 mediates the vascular repair function of ECFCs, future studies toward resolving the complete transcriptional regulatory network in ECFCs will be required to identify additional transcription factors that promote cellular functions that are complementary to migration such as proliferation, differentiation, and angiogenic signaling. This will facilitate the identification of additional epigenetic drugs to be used in combination with HDAC inhibitors to further enhance the therapeutic value of ECFCs.

EXPERIMENTAL PROCEDURES

Cell Culture

Human ECFCs were derived from umbilical cord blood ($n = 12$) obtained after full-term deliveries and cultured essentially as described (Yoder et al., 2007). Informed consent was obtained prior to cord blood collection, and all proce-

dures were approved by the Ottawa Hospital Research Ethics Board (2006460-01H). All experiments were performed with at least three biologically independent ECFC colonies originating from three distinct cord blood donors. See [Supplemental Experimental Procedures](#) for details.

TAL1 Knockdown

The KD of TAL1 was performed by lentivirus-mediated shRNA delivery as previously described (Pali et al., 2011a, 2011b). ECFCs were infected twice at 24 hr interval. The western blot and qRT-PCR showing TAL1 KD were performed 48 hr after the first lentiviral infection (time 0). All phenotypic assays were started at time 0. See [Supplemental Experimental Procedures](#) for details.

Treatment of ECFCs with the HDAC Inhibitor TSA

Paired samples of 70% confluent ECFCs in complete endothelial cell growth medium-2 medium were treated with 100 ng/ml final TSA (cat no. 19-138; Upstate Millipore) or a vehicle control for 24 hr. Cells were washed with PBS prior to harvesting.

Mouse Model of Hindlimb Ischemia

Procedures were performed on 8- or 9-week-old athymic nude CD1 female mice as previously described (Kuraitis et al., 2011) with the approval of the University of Ottawa Animal Care Committee and in accordance with the National Institute of Health Guide for the Care and Use of Laboratory Animals. Unilateral left hindlimb ischemia in mice was induced by ligating the proximal end of the femoral artery using 4-0 silk surgical suture as described in Limbourg et al. (2009). The overlying skin was then closed by a 5-0 proline suture. Cell therapy was administered immediately after skin closure. Specifically, 0.5 million ECFCs that were either nontreated or treated as indicated (infection with lentiviruses or TSA treatment) were resuspended in 50 μ l PBS and delivered by two equivolumetric injections into the adductor muscle downstream of the ligation site using an insulin syringe. The PBS control group received 50 μ l of PBS only.

Laser Doppler Analysis

Blood perfusion analysis was performed preoperatively, immediately after surgery, and at the indicated days postoperation by laser Doppler perfusion imaging (moorLDI2; Moor Instruments). Results are expressed as the ratio of ischemic to nonischemic hindlimb perfusion.

Statistical Analysis

Statistical analyses were performed using Student t test unless otherwise indicated. Bonferroni correction was applied for multiple comparison analyses. Data represent results from at least three independent experiments. Data represent mean \pm SEM. $p < 0.05$ was considered statistically significant.

Gene Expression Profiling on Affymetrix Microarray

Total RNA from three independent ECFC colonies (derived from three distinct cord blood donors), each with or without a TAL1 KD, was analyzed by hybridization to the Affymetrix Human Gene 1.0 ST gene expression microarray. See [Supplemental Experimental Procedures](#) for details.

ChIP

Enrichment of acetylated histone H3 was measured using a native ChIP protocol (Brand et al., 2008). Binding of transcription factors was measured using a crosslink ChIP protocol (Pali et al., 2011b). For qPCR, DNA was quantified with SYBRGreen using a standard curve generated with genomic DNA and was normalized by dividing the amount of the corresponding target in the input fraction. For details on high-throughput DNA-sequencing experiments and analyses see [Supplemental Experimental Procedures](#).

(G) Model of TSA-mediated increase in the migratory function of ECFCs through a TAL1-mediated mechanism. Left: TAL1 activates transcription of migration genes through the recruitment of p300 and subsequent histone acetylation. Right: Inhibition of HDAC activity through TSA treatment displaces the balance toward increasing TAL1-mediated histone acetylation and transcription of migration genes.

For (A), (C), and (D), ChIP-qPCR was performed in ECFCs pretreated with TSA (+TSA) or not (–TSA). ChIP-qPCR values are expressed as the enrichment relative to the no TSA control with error bars corresponding to SD. For (B), qRT-PCR was performed in ECFCs pretreated with TSA (+TSA) or not (–TSA). qRT-PCR values are expressed as the level of transcript relative to the no TSA control with error bars corresponding to SD. See also [Figure S5](#).

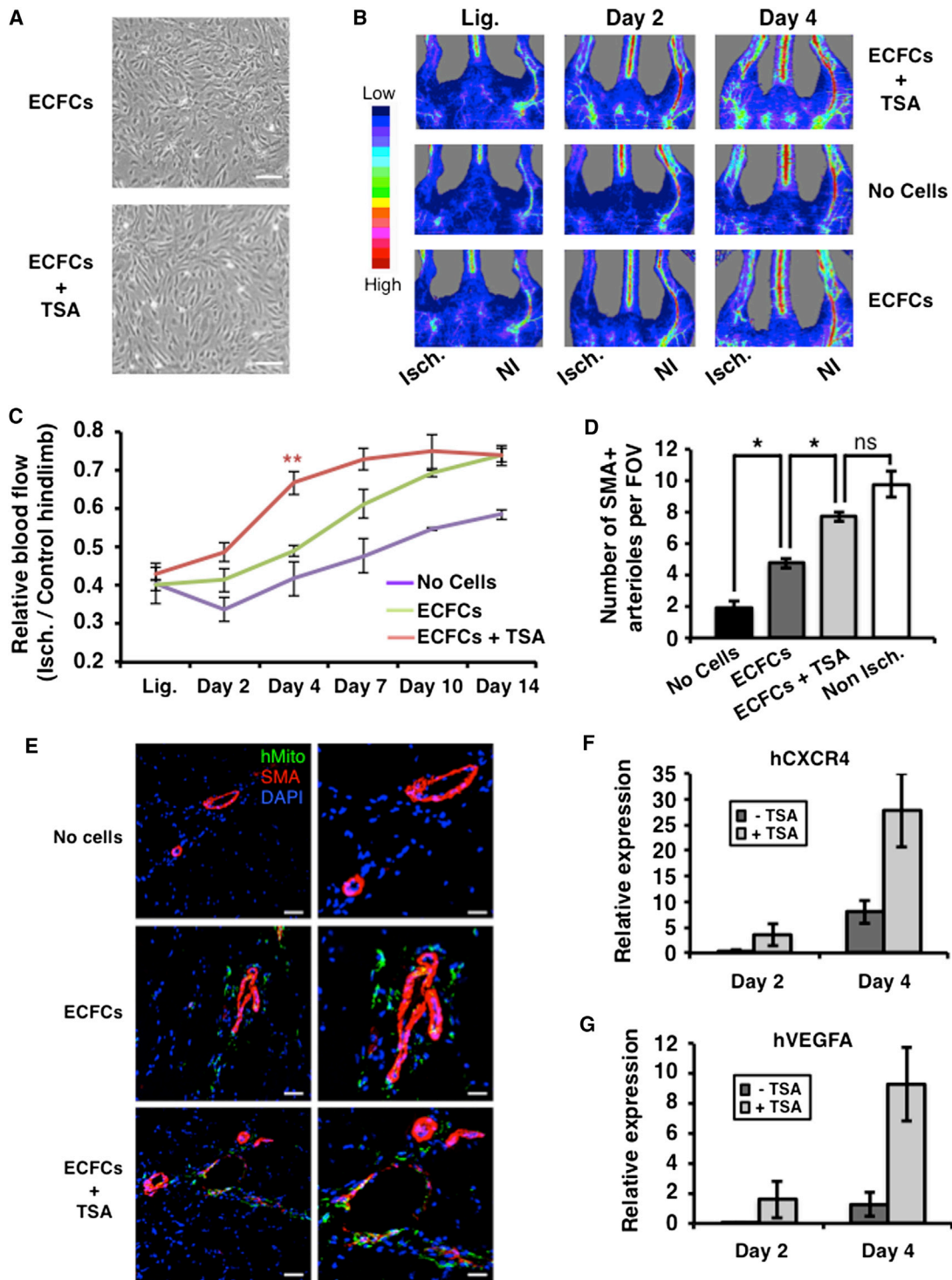


Figure 7. Ex Vivo Treatment with TSA Increases the Efficiency of ECFC-Mediated Revascularization after Ischemia

(A) Representative photomicrographs of ECFCs monolayers with or without TSA treatment (original magnification 100 \times). The scale bar represents 10 μ m. (B and C) Ex vivo treatment with TSA increases the kinetics of blood flow recovery by injected ECFCs in a mouse model of hindlimb ischemia. Relative blood flow was measured by laser Doppler perfusion imaging immediately after induction of hindlimb ischemia (Lig.) and at the indicated time points after injection of PBS (no cells), untreated ECFCs (ECFCs), or ECFCs pretreated with TSA (ECFCs+TSA). For (B), representative laser Doppler images are shown. Isch., ischemic leg; NI, nonischemic leg. For (C), mean values with error bars representing SEM (n = 3 mice for no cells; n = 3 mice for ECFCs; n = 4 mice for ECFCs+TSA). **p = 0.008 for ECFCs+TSA relative to ECFCs-injected mice (indicated on graph). p < 0.05 at all time points for ECFCs+TSA relative to no cells control and at all time points (except day 2) for ECFCs relative to no cells control.

(legend continued on next page)

Antibodies

See [Supplemental Experimental Procedures](#).

qPCR and qRT-PCR Primers

See [Supplemental Experimental Procedures](#).

ACCESSION NUMBERS

The Gene Expression Omnibus accession numbers for the microarray data, ChIP-seq data for TAL1 binding in ECFCs, and ChIP-seq data for TAL1 binding in TSA-treated versus untreated ECFCs reported in this paper are GSE44444, GSE44442, and GSE53423, respectively. All data sets are also saved under the common accession number GSE44546.

SUPPLEMENTAL INFORMATION

Supplemental Information includes Supplemental Experimental Procedures, six figures, and one table and can be found with this article online at <http://dx.doi.org/10.1016/j.stem.2014.03.003>.

ACKNOWLEDGMENTS

We thank C.L. Addison (OHRI) for help with the collagen assay; E. Chernetsova, J.J. Collins, and B. Thebaud (OHRI) for help with immunohistochemistry; Z. Yao (Fred Hutchinson Cancer Research Center, Seattle, WA) for help with bioinformatics analysis; L. Megeney (OHRI) for reagents; and M. Rudnicki and B. Thebaud (OHRI) for critically reading the manuscript. Affymetrix microarray analysis was done at the StemCore Laboratories (Ottawa, ON). High-throughput DNA sequencing was done at the McGill University and Génome Québec Innovation Centre (Montréal, QC). This project was funded with grants from the Canadian Institutes of Health Research (MOP-82813 to M.B.); the Department of Medicine, University of Ottawa (to D.A.); and the Heart & Stroke Foundation of Canada (GIA-000225 to E.J.S.). C.G.P. is supported in part by the Cardiovascular Repair using Enhanced Stem Cell Therapy program. B.V. is supported by a graduate scholarship from CIHR. S.F. is supported by the Cushing Fund. M.B. holds the Canadian Research Chair in the Regulation of Gene Expression, and D.A. holds a New Investigator Award from CIHR.

Received: March 15, 2013

Revised: January 8, 2014

Accepted: March 11, 2014

Published: May 1, 2014

REFERENCES

Asahara, T., Murohara, T., Sullivan, A., Silver, M., van der Zee, R., Li, T., Witzenbichler, B., Schatteman, G., and Isner, J.M. (1997). Isolation of putative progenitor endothelial cells for angiogenesis. *Science* *275*, 964–967.

Au, P., Daheron, L.M., Duda, D.G., Cohen, K.S., Tyrrell, J.A., Lanning, R.M., Fukumura, D., Scadden, D.T., and Jain, R.K. (2008). Differential in vivo potential of endothelial progenitor cells from human umbilical cord blood and adult peripheral blood to form functional long-lasting vessels. *Blood* *111*, 1302–1305.

Bouvard, C., Gafsou, B., Dizier, B., Galy-Fauroux, I., Lokajczyk, A., Boisson-Vidal, C., Fischer, A.M., and Helley, D. (2010). $\alpha 6$ -integrin subunit plays a major role in the proangiogenic properties of endothelial progenitor cells. *Arterioscler. Thromb. Vasc. Biol.* *30*, 1569–1575.

Brand, M., Rampalli, S., Chaturvedi, C.P., and Dilworth, F.J. (2008). Analysis of epigenetic modifications of chromatin at specific gene loci by native chromatin immunoprecipitation of nucleosomes isolated using hydroxyapatite chromatography. *Nat. Protoc.* *3*, 398–409.

Bruhl, T., Urbich, C., Aicher, D., Acker-Palmer, A., Zeiher, A.M., and Dimmeler, S. (2004). Homeobox A9 transcriptionally regulates the EphB4 receptor to modulate endothelial cell migration and tube formation. *Circ. Res.* *94*, 743–751.

Callum, K., and Bradbury, A. (2000). ABC of arterial and venous disease: Acute limb ischaemia. *BMJ* *320*, 764–767.

Ceradini, D.J., Kulkarni, A.R., Callaghan, M.J., Tepper, O.M., Bastidas, N., Kleinman, M.E., Capla, J.M., Galiano, R.D., Levine, J.P., and Gurtner, G.C. (2004). Progenitor cell trafficking is regulated by hypoxic gradients through HIF-1 induction of SDF-1. *Nat. Med.* *10*, 858–864.

Chetty, R., Dada, M.A., Boshoff, C.H., Comley, M.A., Biddolph, S.C., Schneider, J.W., Mason, D.Y., Pulford, K.A., and Gatter, K.C. (1997). TAL-1 protein expression in vascular lesions. *J. Pathol.* *181*, 311–315.

Costa, G., Mazan, A., Gandillet, A., Pearson, S., Lacaud, G., and Kouskoff, V. (2012). SOX7 regulates the expression of VE-cadherin in the haemogenic endothelium at the onset of haematopoietic development. *Development* *139*, 1587–1598.

Creager, M.A., Kaufman, J.A., and Conte, M.S. (2012). Clinical practice. Acute limb ischemia. *N. Engl. J. Med.* *366*, 2198–2206.

De Val, S., and Black, B.L. (2009). Transcriptional control of endothelial cell development. *Dev. Cell* *16*, 180–195.

Deleuze, V., Chalhou, E., El-Hajj, R., Dohet, C., Le Clech, M., Couraud, P.O., Huber, P., and Mathieu, D. (2007). TAL-1/SCL and its partners E47 and LMO2 up-regulate VE-cadherin expression in endothelial cells. *Mol. Cell. Biol.* *27*, 2687–2697.

Dooley, K.A., Davidson, A.J., and Zon, L.I. (2005). Zebrafish scl functions independently in hematopoietic and endothelial development. *Dev. Biol.* *277*, 522–536.

Fadini, G.P., Losordo, D., and Dimmeler, S. (2012). Critical reevaluation of endothelial progenitor cell phenotypes for therapeutic and diagnostic use. *Circ. Res.* *110*, 624–637.

Fong, A.P., Yao, Z., Zhong, J.W., Cao, Y., Ruzzo, W.L., Gentleman, R.C., and Tapscott, S.J. (2012). Genetic and epigenetic determinants of neurogenesis and myogenesis. *Dev. Cell* *22*, 721–735.

Fujiwara, T., O'Geen, H., Keles, S., Blahnik, K., Linnemann, A.K., Kang, Y.A., Choi, K., Farnham, P.J., and Bresnick, E.H. (2009). Discovering hematopoietic mechanisms through genome-wide analysis of GATA factor chromatin occupancy. *Mol. Cell* *36*, 667–681.

Grunewald, M., Avraham, I., Dor, Y., Bachar-Lustig, E., Itin, A., Jung, S., Chimenti, S., Landsman, L., Abramovitch, R., and Keshet, E. (2006). VEGF-induced adult neovascularization: recruitment, retention, and role of accessory cells. *Cell* *124*, 175–189.

(D) Increased arteriole density in the ischemic muscle of mice injected with TSA-treated ECFCs. Quantification of SMA⁺ vessels 4 days after ECFCs transplantation. Results are expressed as the number of SMA⁺ vessels per FOV \pm SEM. * $p < 0.01$. ns, nonsignificant.

(E) Human ECFCs with or without TSA pretreatment engraft into the vasculature of ischemic muscle. Immunostaining was performed on ischemic muscle cryosections with a human-specific mitochondrial Ab (hMito, green) and a murine-specific smooth muscle actin Ab (SMA, red) 4 days after injection of PBS (no cells), ECFCs pretreated with TSA (+TSA) or untreated ECFCs. Nuclei were stained with DAPI (blue). Left panels, scale bar: 50 μ m. Right panels, scale bar: 25 μ m.

(F) TSA-treated ECFCs express higher levels of hCXCR4 in the ischemic muscle. qRT-PCR was performed on RNA isolated from whole dissected ischemic muscles injected with PBS or with ECFCs pretreated with TSA (+TSA) or not (–TSA) using primers specific for human CXCR4 (hCXCR4). qRT-PCR values for hCXCR4 are normalized to the total number of engrafted ECFCs per mouse muscle (quantified by measuring human Alu repeats as previously described [Lee et al., 2006] and normalized to rodent GAPDH \pm SEM [$n = 3$ mice per group]). No hCXCR4 was detected in mice injected with PBS.

(G) Higher expression of hVEGFA in the ischemic muscle injected with TSA-treated ECFCs. Expression of human VEGFA (hVEGFA) was determined by qRT-PCR as described for hCXCR4 in (F).

See also [Figure S6](#).

- Huang, S., Qiu, Y., Stein, R.W., and Brandt, S.J. (1999). p300 functions as a transcriptional coactivator for the TAL1/SCL oncoprotein. *Oncogene* *18*, 4958–4967.
- Huang, S., Qiu, Y., Shi, Y., Xu, Z., and Brandt, S.J. (2000). P/CAF-mediated acetylation regulates the function of the basic helix-loop-helix transcription factor TAL1/SCL. *EMBO J.* *19*, 6792–6803.
- Ingram, D.A., Mead, L.E., Tanaka, H., Meade, V., Fenoglio, A., Mortell, K., Pollok, K., Ferkowicz, M.J., Gilley, D., and Yoder, M.C. (2004). Identification of a novel hierarchy of endothelial progenitor cells using human peripheral and umbilical cord blood. *Blood* *104*, 2752–2760.
- Kallianpur, A.R., Jordan, J.E., and Brandt, S.J. (1994). The SCL/TAL-1 gene is expressed in progenitors of both the hematopoietic and vascular systems during embryogenesis. *Blood* *83*, 1200–1208.
- Khandekar, M., Brandt, W., Zhou, Y., Dagenais, S., Glover, T.W., Suzuki, N., Shimizu, R., Yamamoto, M., Lim, K.C., and Engel, J.D. (2007). A Gata2 intronic enhancer confers its pan-endothelia-specific regulation. *Development* *134*, 1703–1712.
- Kuraitis, D., Hou, C., Zhang, Y., Vulesevic, B., Sofrenovic, T., McKee, D., Sharif, Z., Ruel, M., and Suuronen, E.J. (2011). Ex vivo generation of a highly potent population of circulating angiogenic cells using a collagen matrix. *J. Mol. Cell. Cardiol.* *51*, 187–197.
- Lancrin, C., Sroczyńska, P., Stephenson, C., Allen, T., Kouskoff, V., and Lacaud, G. (2009). The haemangioblast generates haematopoietic cells through a haemogenic endothelium stage. *Nature* *457*, 892–895.
- Lee, R.H., Hsu, S.C., Munoz, J., Jung, J.S., Lee, N.R., Pochampally, R., and Prockop, D.J. (2006). A subset of human rapidly self-renewing marrow stromal cells preferentially engraft in mice. *Blood* *107*, 2153–2161.
- Leeper, N.J., Hunter, A.L., and Cooke, J.P. (2010). Stem cell therapy for vascular regeneration: adult, embryonic, and induced pluripotent stem cells. *Circulation* *122*, 517–526.
- Limbourg, A., Korff, T., Napp, L.C., Schaper, W., Drexler, H., and Limbourg, F.P. (2009). Evaluation of postnatal arteriogenesis and angiogenesis in a mouse model of hind-limb ischemia. *Nat. Protoc.* *4*, 1737–1746.
- Lin, Y., Weisdorf, D.J., Solovey, A., and Hebbel, R.P. (2000). Origins of circulating endothelial cells and endothelial outgrowth from blood. *J. Clin. Invest.* *105*, 71–77.
- Liu, J., Huang, J., Yao, W.Y., Ben, Q.W., Chen, D.F., He, X.Y., Li, L., and Yuan, Y.Z. (2012). The origins of vascularization in tumors. *Front Biosci (Landmark Ed)* *17*, 2559–2565.
- McLean, C.Y., Bristol, D., Hiller, M., Clarke, S.L., Schaar, B.T., Lowe, C.B., Wenger, A.M., and Bejerano, G. (2010). GREAT improves functional interpretation of cis-regulatory regions. *Nat. Biotechnol.* *28*, 495–501.
- Melero-Martin, J.M., Khan, Z.A., Picard, A., Wu, X., Paruchuri, S., and Bischoff, J. (2007). In vivo vasculogenic potential of human blood-derived endothelial progenitor cells. *Blood* *109*, 4761–4768.
- Moubarik, C., Guillet, B., Youssef, B., Codaccioni, J.L., Piercecchi, M.D., Sabatier, F., Lionel, P., Dou, L., Foucault-Bertaud, A., Velly, L., et al. (2011). Transplanted late outgrowth endothelial progenitor cells as cell therapy product for stroke. *Stem Cell Rev.* *7*, 208–220.
- Palii, C.G., Pasha, R., and Brand, M. (2011a). Lentiviral-mediated knockdown during ex vivo erythropoiesis of human hematopoietic stem cells. *J. Vis. Exp.* (53), pii: 2813.
- Palii, C.G., Perez-Iratxeta, C., Yao, Z., Cao, Y., Dai, F., Davison, J., Atkins, H., Allan, D., Dilworth, F.J., Gentleman, R., et al. (2011b). Differential genomic targeting of the transcription factor TAL1 in alternate haematopoietic lineages. *EMBO J.* *30*, 494–509.
- Patterson, L.J., Gering, M., and Patient, R. (2005). Scl is required for dorsal aorta as well as blood formation in zebrafish embryos. *Blood* *105*, 3502–3511.
- Reinisch, A., Hofmann, N.A., Obenauf, A.C., Kashofer, K., Rohde, E., Schallmoser, K., Flicker, K., Lanzer, G., Linkesch, W., Speicher, M.R., and Strunk, D. (2009). Humanized large-scale expanded endothelial colony-forming cells function in vitro and in vivo. *Blood* *113*, 6716–6725.
- Rössig, L., Urbich, C., Brühl, T., Dernbach, E., Heeschen, C., Chavakis, E., Sasaki, K., Aicher, D., Diehl, F., Seeger, F., et al. (2005). Histone deacetylase activity is essential for the expression of HoxA9 and for endothelial commitment of progenitor cells. *J. Exp. Med.* *207*, 1825–1835.
- Saif, J., Schwarz, T.M., Chau, D.Y., Henstock, J., Sami, P., Leicht, S.F., Hermann, P.C., Alcalá, S., Mulero, F., Shakesheff, K.M., et al. (2010). Combination of injectable multiple growth factor-releasing scaffolds and cell therapy as an advanced modality to enhance tissue neovascularization. *Arterioscler. Thromb. Vasc. Biol.* *30*, 1897–1904.
- Salvucci, O., and Tosato, G. (2012). Essential roles of EphB receptors and EphrinB ligands in endothelial cell function and angiogenesis. *Adv. Cancer Res.* *114*, 21–57.
- Schwarz, T.M., Leicht, S.F., Radic, T., Rodriguez-Araboalaza, I., Hermann, P.C., Berger, F., Saif, J., Böcker, W., Ellwart, J.W., Aicher, A., and Heeschen, C. (2012). Vascular incorporation of endothelial colony-forming cells is essential for functional recovery of murine ischemic tissue following cell therapy. *Arterioscler. Thromb. Vasc. Biol.* *32*, e13–e21.
- Shivdasani, R.A., Mayer, E.L., and Orkin, S.H. (1995). Absence of blood formation in mice lacking the T-cell leukaemia oncoprotein tal-1/SCL. *Nature* *373*, 432–434.
- Soler, E., Andrieu-Soler, C., de Boer, E., Bryne, J.C., Thongjuea, S., Stadhouders, R., Palstra, R.J., Stevens, M., Kockx, C., van Ijcken, W., et al. (2010). The genome-wide dynamics of the binding of Ldb1 complexes during erythroid differentiation. *Genes Dev.* *24*, 277–289.
- Van Handel, B., Montel-Hagen, A., Sasidharan, R., Nakano, H., Ferrari, R., Boogerd, C.J., Schredelseker, J., Wang, Y., Hunter, S., Org, T., et al. (2012). Scl represses cardiomyogenesis in prospective hemogenic endothelium and endocardium. *Cell* *150*, 590–605.
- Visvader, J.E., Fujiwara, Y., and Orkin, S.H. (1998). Unsuspected role for the T-cell leukemia protein SCL/tal-1 in vascular development. *Genes Dev.* *12*, 473–479.
- Wang, Z., Zang, C., Cui, K., Schones, D.E., Barski, A., Peng, W., and Zhao, K. (2009). Genome-wide mapping of HATs and HDACs reveals distinct functions in active and inactive genes. *Cell* *138*, 1019–1031.
- Wilson, N.K., Foster, S.D., Wang, X., Knezevic, K., Schütte, J., Kaimakis, P., Chilarska, P.M., Kinston, S., Ouwehand, W.H., Dzierzak, E., et al. (2010). Combinatorial transcriptional control in blood stem/progenitor cells: genome-wide analysis of ten major transcriptional regulators. *Cell Stem Cell* *7*, 532–544.
- Yoder, M.C. (2012). Human endothelial progenitor cells. *Cold Spring Harb. Perspect. Med.* *2*, a006692.
- Yoder, M.C., Mead, L.E., Prater, D., Krier, T.R., Mroueh, K.N., Li, F., Krasich, R., Temm, C.J., Prchal, J.T., and Ingram, D.A. (2007). Redefining endothelial progenitor cells via clonal analysis and hematopoietic stem/progenitor cell principals. *Blood* *109*, 1801–1809.
- Zeng, L., and Zhou, M.M. (2002). Bromodomain: an acetyl-lysine binding domain. *FEBS Lett.* *513*, 124–128.
- Ziebart, T., Yoon, C.H., Trepels, T., Wietelmann, A., Braun, T., Kiessling, F., Stein, S., Grez, M., Ihling, C., Muhly-Reinholz, M., et al. (2008). Sustained persistence of transplanted proangiogenic cells contributes to neovascularization and cardiac function after ischemia. *Circ. Res.* *103*, 1327–1334.

Cell Stem Cell, Volume 14

Supplemental Information

**Trichostatin A Enhances Vascular Repair by
Injected Human Endothelial Progenitors through
Increasing the Expression of TAL1-Dependent Genes**

Carmen G. Pali, Branka Vulesevic, Sylvain Fraineau, Erinija Pranckeviciene, Alexander J. Griffith, Alphonse Chu, Hervé Faralli, Yuhua Li, Brian McNeill, Jie Sun, Theodore J. Perkins, F. Jeffrey Dilworth, Carol Perez-Iratxeta, Erik J. Suuronen, David Allan, and Marjorie Brand

SUPPLEMENTAL INFORMATION

Supplemental Figures

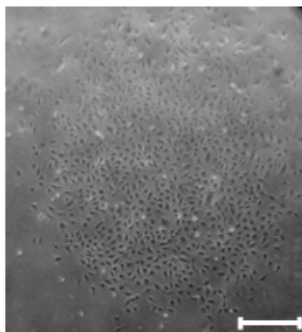
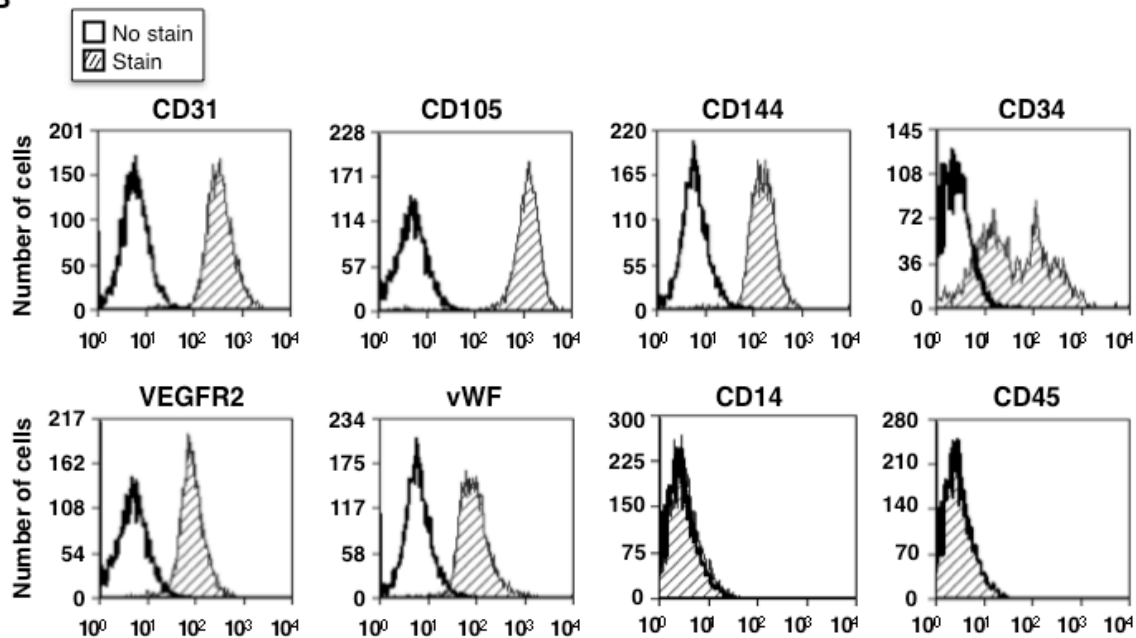
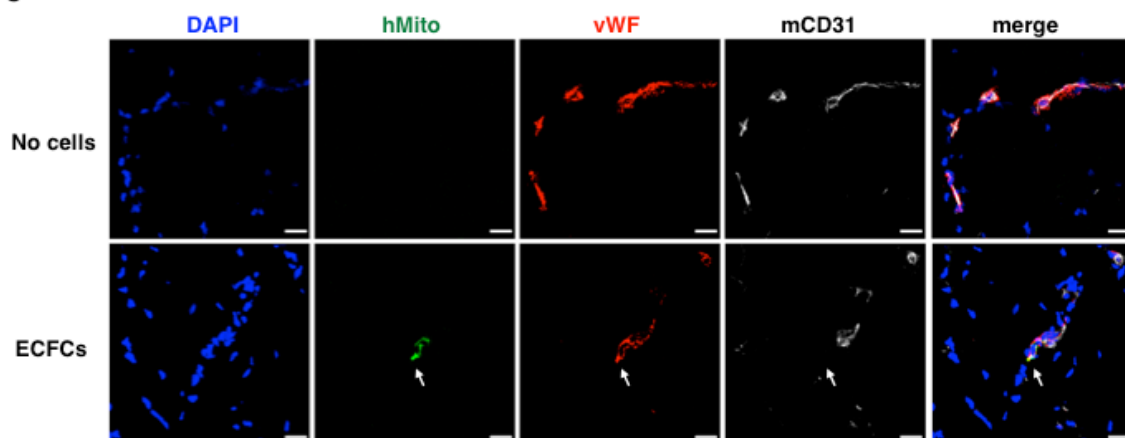
A**B****C**

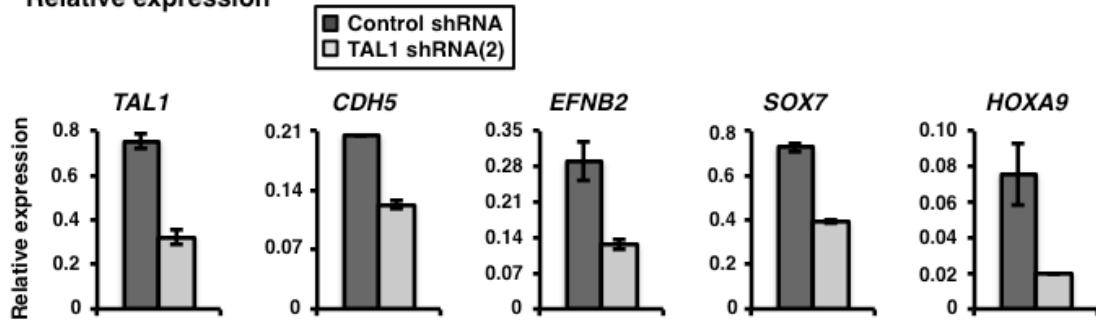
Figure S1 (related to Figure 1): Phenotypic characterization of cord-blood-derived human endothelial colony-forming cells (ECFCs)

(A) Representative phase contrast image of an individual ECFC colony. Scale bar: 50 μm

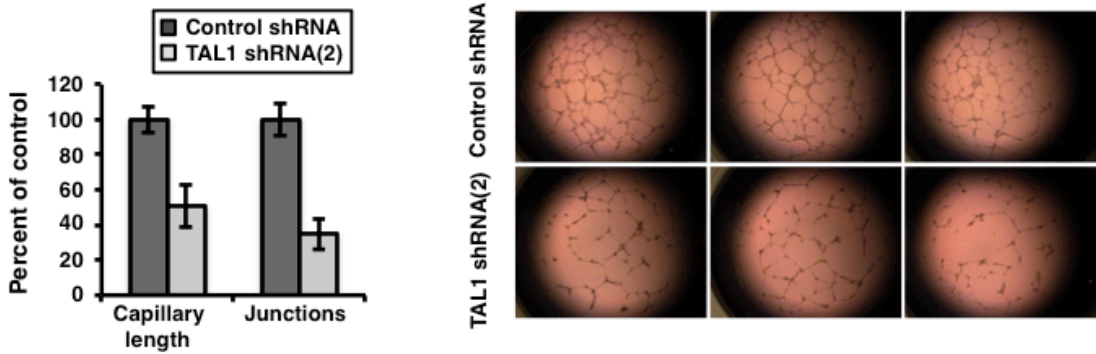
(B) Representative flow cytometry histograms of ECFCs at passage 3. These cells express the following endothelial cell surface antigens: CD31 (platelet/endothelial cell adhesion molecule 1), CD105 (endoglin), CD144 (vascular endothelial cadherin), VEGFR2 (vascular endothelial growth factor receptor 2), vWF (endothelial von Willebrand factor), as well as the hematopoietic and endothelial cell surface antigen CD34, but not the hematopoietic-specific cell surface antigens CD14 and CD45. In the manuscript, we have used only ECFC colonies at passage 3, and verified that they all present highly similar phenotypic characteristics.

(C) Representative example of a blood vessel containing both human and mouse endothelial cells in the ischemic muscle of a mouse injected with ECFCs. Immunostaining was performed on ischemic muscles cryosections with a human-specific mitochondrial antibody (hMito, green), an antibody that recognizes both human and mouse vWF (vWF, red) and a mouse-specific CD31 antibody (mCD31, white) after injection of PBS (no cells) or ECFCs, as indicated. Nuclei were stained with DAPI (blue). The arrow indicates a blood vessel containing human endothelial cells with overlapping staining for hMito and vWF but negative for staining with mCD31 antibody. Scale bar: 20 μm .

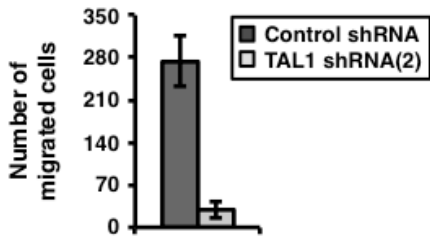
A Relative expression



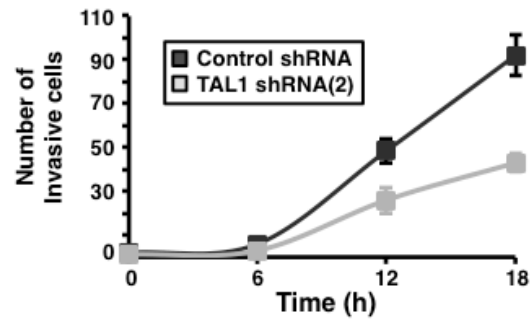
B Capillary-like structure formation



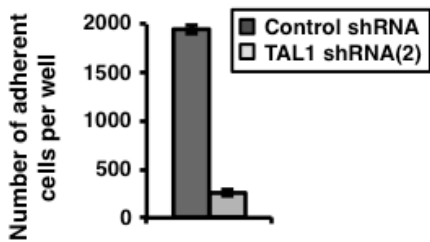
C Chemotaxis (SDF-1)



D Migration



E Adhesion



F Arteriole density in ischemic muscle

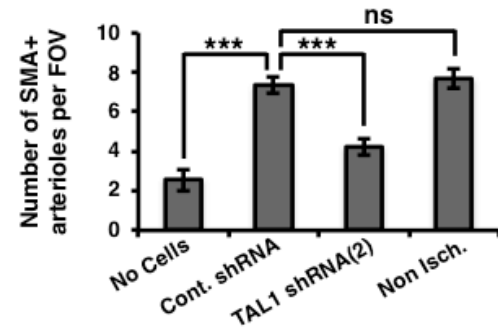


Figure S2 (related to Figure 3): Phenotypic analyses after TAL1 KD with a second anti-TAL1 shRNA (shRNA(2))

(A) Transcripts levels of TAL1 and its target genes are decreased in ECFCs after lentiviral delivery of anti-TAL1 shRNA(2) relative to a control scrambled shRNA. RT-qPCR values are expressed relative to the internal control *GAPDH* (n=3). (B) TAL1 KD with shRNA(2) leads to a profound defect in capillary-like structure formation after ECFCs plating on Matrigel. Left panel, Quantification of capillary-like structures length, and number of junctions by automatic counting with the AngioQuant software (version 1.33). Data are expressed as percentages of values obtained for ECFCs infected with a control shRNA. Right panel, Representative images (n=3). (C) TAL1 KD with shRNA(2) decreases ECFCs migration by chemotaxis towards SDF-1 as measured by a modified Boyden chamber migration assay (n=3). (D) TAL1 KD with shRNA(2) decreases ECFCs migration as measured by gap closure assay (n=3). (E) TAL1 KD with shRNA(2) decreases ECFCs adhesion on a 24-well plate (n=3). (A-E) Error bars represent SD of biological triplicates. (F) TAL1 KD with shRNA(2) decreases the vascular repair capacity of ECFCs in a mouse model of hindlimb ischemia. Arteriole density was measured by counting the number of SMA⁺ vessels per field of view (FOV). Results are expressed as the mean +/- SEM. ***p < 0.001; ns, non-significant.

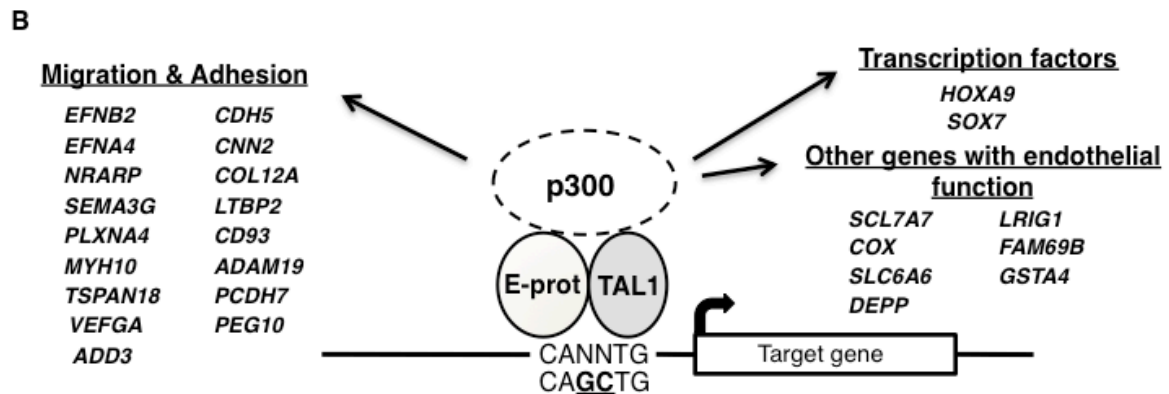
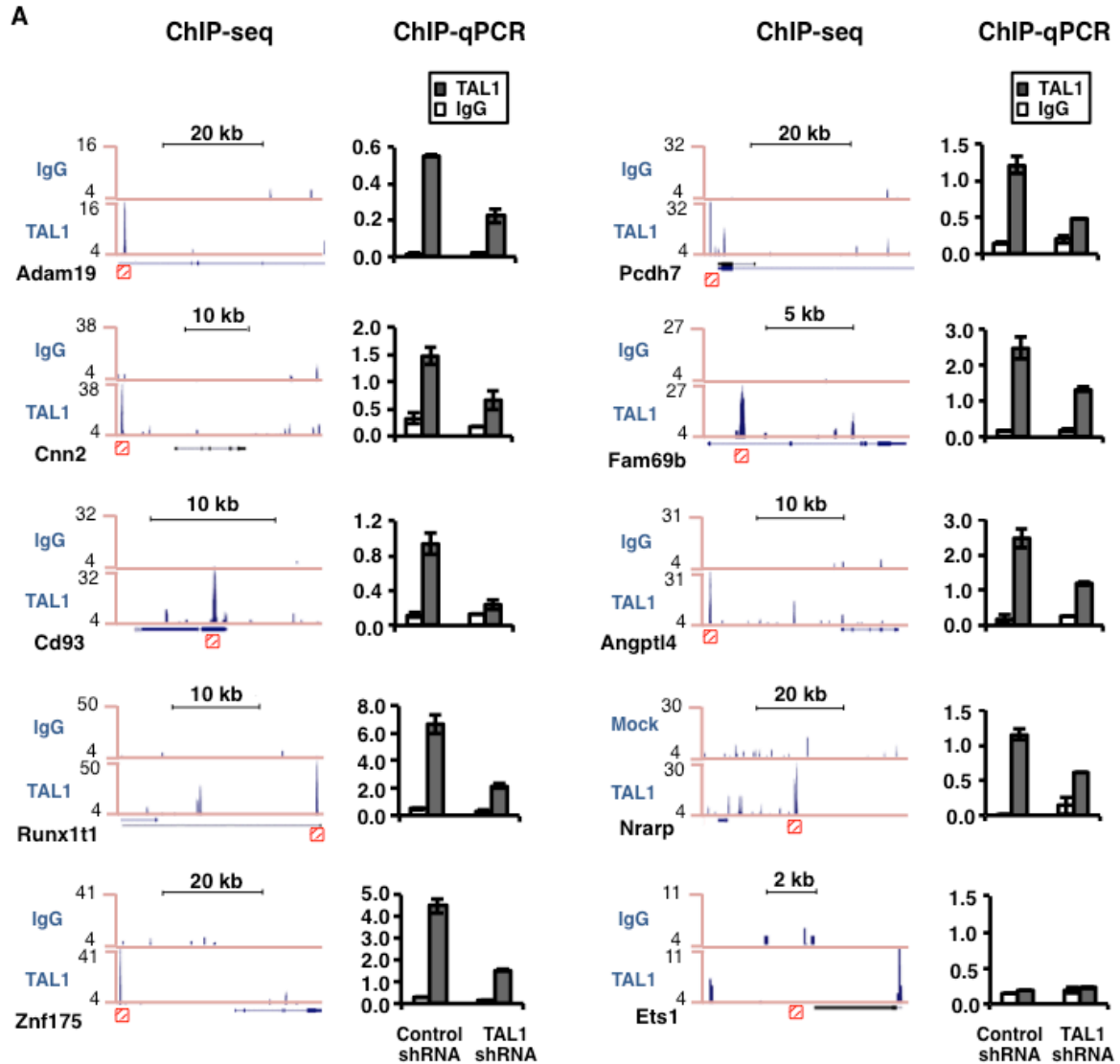


Figure S3 (related to Figure 4): Validation of TAL1 ChIP-sequencing results by ChIP-qPCR

(A) TAL1 binding obtained by ChIP-seq was verified by independent ChIP-qPCR experiments performed in the presence of normal (control shRNA) or reduced (TAL1 shRNA) levels of TAL1 using a TAL1 Ab or normal IgG as indicated. A decrease in TAL1 binding signal upon TAL1 knockdown validates the ChIP specificity. ChIP-seq density plots were generated from raw data and loaded into the UCSC Genome Browser as custom tracks. ChIP-qPCR values are expressed as fractions of input with error bars corresponding to SD. The positions of primer pairs used for qPCR are indicated by a red hatched square.

(B) Representative TAL1-target genes identified by ChIP-seq and gene expression profiling upon TAL1 KD in ECFCs. TAL1 activated genes in ECFCs comprise effector genes that increase cell migration and adhesion as well as transcription factor genes.

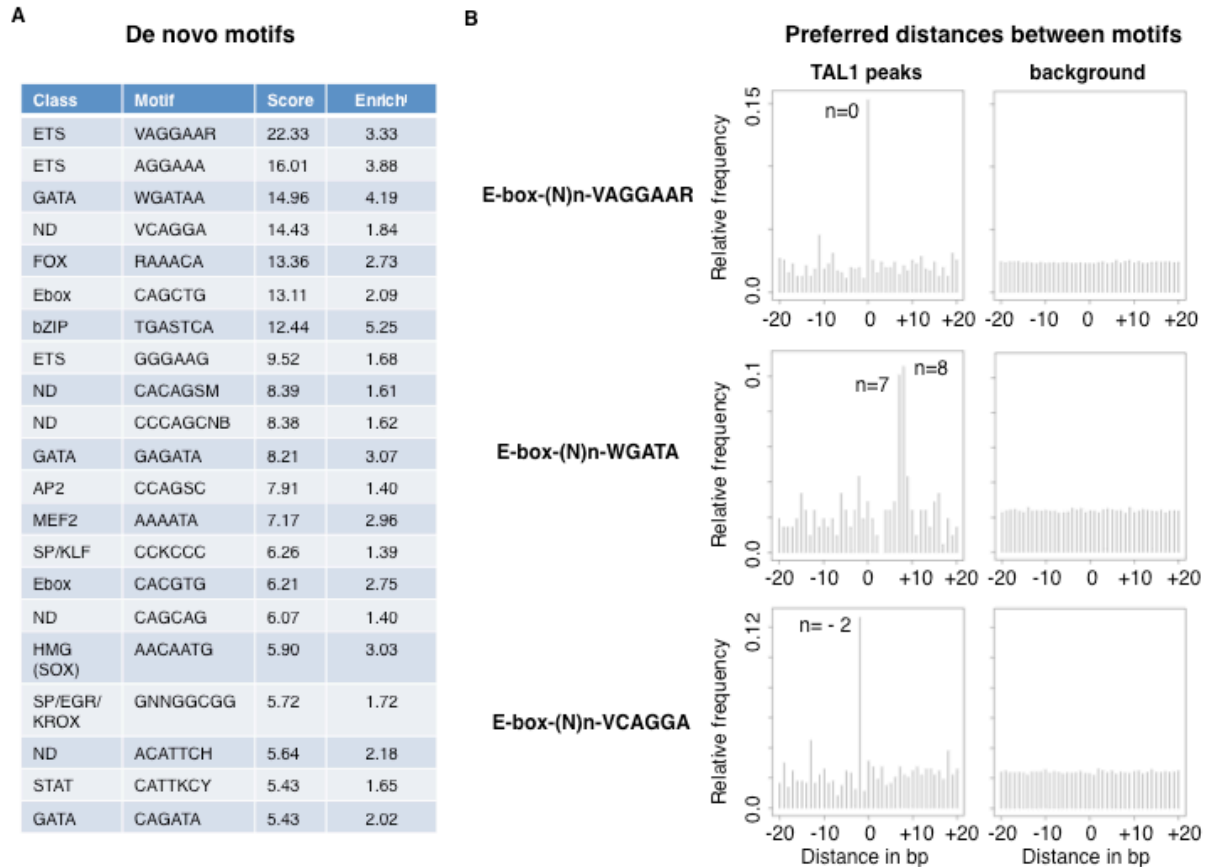


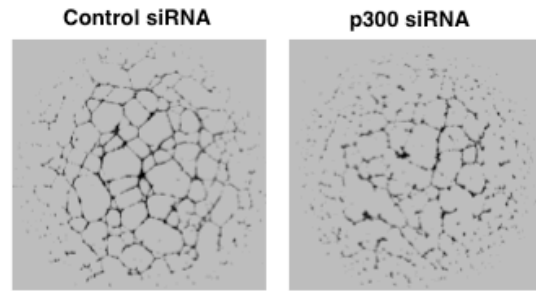
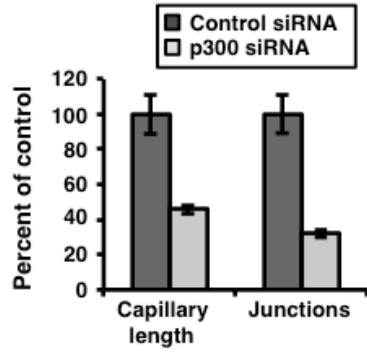
Figure S4 (related to Figure 4): DNA motifs overrepresented under peaks of TAL1 binding

(A) DNA motifs that are overrepresented under peaks of TAL1 binding were identified using the MotifRG Bioconductor package for discriminative motif discovery (Fong et al., 2012; Pali et al., 2011b). Motifs scores are defined as z-values of logistic regression. Classes of motifs were identified using STAMP (Parks and Beiko, 2010) against the TRANSFAC_Fams database. See Figure 4A for logo representations.

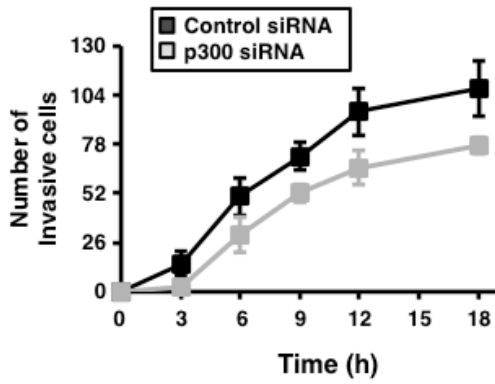
(B) Composite motifs that are overrepresented under peaks of TAL1 binding were identified by measuring the relative frequency of preferred distances (in bp)

between E-box and the indicated DNA motifs (identified in panel A). The x-axis corresponds to the distance (in bps) between the two motifs. See Figure 4B for logo representations.

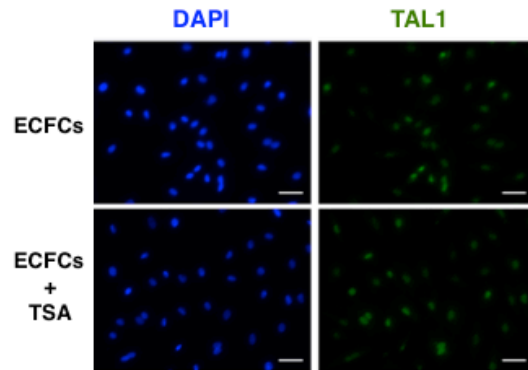
A Capillary-like structure formation



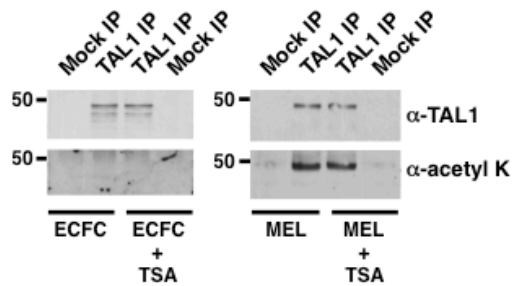
B Migration



C



D



E

Comparison of TAL1 ChIP-seq data sets		PCC
ECFC + TSA	ECFC - TSA	0.96
Erythroid Replicate 1	Erythroid Replicate 2	0.92
Jurkat Replicate 1	Jurkat Replicate 2	0.87
Erythroid	Jurkat	0.40
Erythroid	CCRF-CEM	0.27
ECFC	Jurkat	0.11
ECFC	Erythroid	0.09
ECFC	CCRF-CEM	0.06

Figure S5 (related to Figure 6): Measuring the effects of p300 knockdown and TSA treatment in ECFCs

(A,B) Knockdown (KD) of p300 in ECFCs impairs *in vitro* angiogenesis.

(A) p300 KD with siRNA leads to a profound defect in capillary-like structure formation after ECFCs plating on Matrigel. Left panel, Quantification of capillary-like structures length, and number of junctions by automatic counting with the AngioQuant software (version 1.33). Data are expressed as percentages of values obtained for ECFCs transfected with a control siRNA. Right panel, Representative images of capillary-like networks stained with calcein. (B) p300 KD with siRNA decreases ECFCs migration as measured by gap closure assay (n=3). (A,B) Error bars represent SD of biological triplicates.

(C-E) TSA treatment of ECFCs does not change TAL1 cellular localization, its acetylation status or its genome-wide binding.

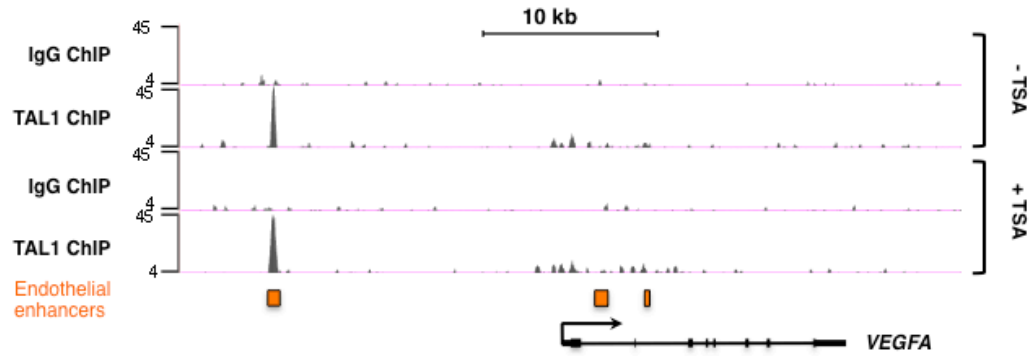
(C) TAL1 cellular localization upon TSA treatment was assessed by immunocytochemistry on fixed ECFCs using an anti-TAL1 Ab (green). Nuclei were stained with DAPI (blue). Scale bar: 50 μ m.

(D) The acetylation status of TAL1 upon TSA treatment was assessed in ECFCs and MEL cells by Western blot following TAL1 immunoprecipitation (IP). A mock IP using normal IgG was used as a negative control. Molecular masses (Left; in kDa) and Abs used for Western blot (Right) are indicated.

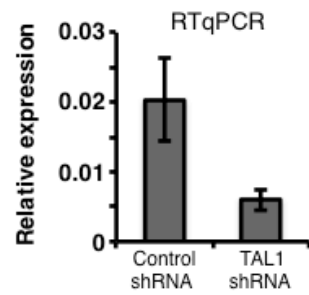
(E) Comparative analyses of TAL1 genome-wide binding were performed by calculating the Pearson's linear correlation coefficient (PCC) for multiple pairs of

TAL1 ChIP-seq data sets in various cellular environments (i.e. ECFCs, erythroid cells, and the T-ALL cell lines Jurkat and CCRF-CEM) as indicated. Comparison of ChIP-seq data sets of TAL1 binding in identical cellular environments (i.e. ChIP-seq replicates) serves as positive controls (PCC close to 1) while comparison of ChIP-seq data sets of TAL1 binding in distant cellular environments serves as a control for divergence (PCC close to 0). ChIP-seq datasets used were as follow: ECFC (this study), Erythroid and Jurkat (Palii et al., 2011b), CCRF-CEM (Sanda et al., 2012).

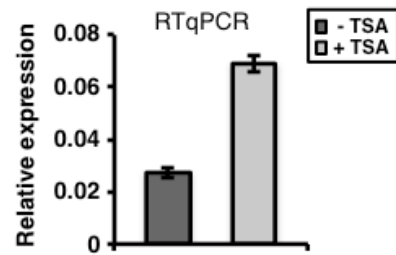
A TAL1 binding to the *VEGFA* locus before and after TSA treatment



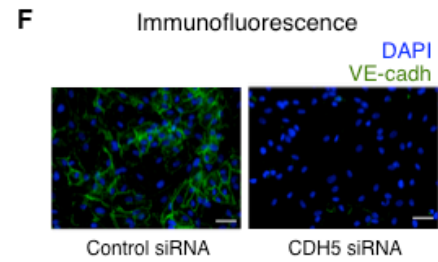
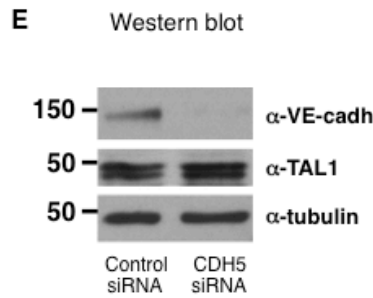
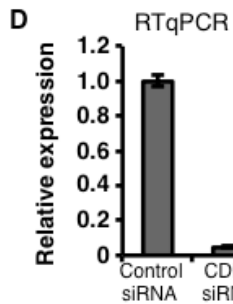
B TAL1 KD decreases *VEGFA* expression



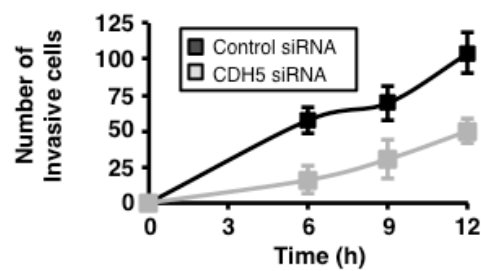
C TSA increases *VEGFA* expression



Knockdown of the TAL1-target gene *CDH5* (VE-cadherin) in TSA-treated ECFCs



G Migration



H Doppler

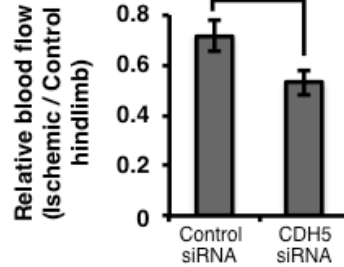


Figure S6 (related to Figure 7): Modulation of TAL1-target genes by TSA-treatment of ECFCs.

(A) TAL1 binding to the *VEGFA* locus is not changed upon TSA treatment of ECFCs. TAL1 binds to an active endothelial enhancer (identified by ChromHMM (Ernst and Kellis, 2012)-highlighted in orange) upstream of the *VEGFA* gene before and after TSA treatment. TAL1 and control (IgG) ChIP-seq density plots were generated from raw data and loaded into the UCSC Genome Browser as custom tracks. (B) TAL1 KD decreases *VEGFA* expression in ECFCs. (C) *VEGFA* expression is up-regulated in ECFCs upon TSA treatment. (B,C) RT-qPCR values are expressed relative to the internal control *GAPDH* with error bars corresponding to SD. (D-H) KD of the TAL1-target gene *CDH5* (VE-cadherin) in TSA-treated ECFCs recapitulates the effects of TAL1 KD on cell migration and blood flow recovery in the mouse model of hindlimb ischemia. *CDH5* levels are decreased in ECFCs after transfection of anti-*CDH5* siRNA relative to a control siRNA, as measured by RTqPCR (D), western blot (E) and immunostaining (F). (G) *CDH5* KD decreases ECFCs migration as measured by gap closure assay. Results are expressed as the number of ECFCs that have migrated into a “cell-free” zone (n=3). (H) ECFCs with a KD of *CDH5* are less efficient than control ECFCs in improving blood perfusion recovery in a mouse model of hindlimb ischemia. Relative blood flow (ischemic / nonischemic hindlimb) was measured by laser Doppler perfusion imaging after injection of

ECFCs transfected with an anti-CDH5 siRNA or a control siRNA. Results are expressed as the mean \pm SEM (3 mice per group). *p = 0.04.

(E) Molecular masses (in kDa) are indicated on the left

(F) Immunocytochemistry was performed on fixed ECFCs using an anti-VE-cadh.

Ab (green). Nuclei were stained with DAPI (blue). Scale bar: 50 μ m.

Table S1 (related to Figures 4 and 5):

(A) Full list of Gene Ontology Biological Process categories, Panther Pathways and MGI Expression categories that are significantly enriched among TAL1 target genes. This analysis was performed using the Genomic Regions Enrichment of Annotation Tool (GREAT) v.2.02 with default parameters (McLean et al., 2010).

(B) List of genes that change their expression upon TAL1 KD (identified by gene expression microarray).

(C) List of TAL1-regulated genes defined as the genes that are differentially expressed upon TAL1 KD (identified by gene expression microarray) and have at least one TAL1 peak within a 100 kb distance.

Supplemental Experimental Procedures

Cell Culture

Human ECFCs were derived from umbilical cord blood (UCB) (n=12) obtained after full-term deliveries, and cultured essentially as described (Yoder et al., 2007). Mononuclear cells (MNCs) were isolated from UCB by Ficoll density gradient centrifugation (GE Healthcare), resuspended into complete EGM-2 medium (EBM-2 medium (Lonza, cc-3156) supplemented with EGM-2 SingleQuot Kit Supplements and Growth Factors (Lonza, cc-4176), and 10% FBS), and seeded onto 6-well plates (CellBIND, Corning). The medium was changed daily for 7 days and then, every other day. Individual ECFC colonies (Figure S1A) emerged 4 to 16 days after seeding and were re-plated separately. Complete EGM-2 medium was changed every other day. Individual ECFCs colonies were analyzed by flow cytometry for the expression of endothelial and hematopoietic cell surface markers. All experiments were performed with individual ECFCs colonies at passage 3. All experiments were performed with at least 3 biologically independent ECFC colonies originating from 3 distinct cord blood donors.

MEL cells (clone 745) were grown and differentiated towards the erythroid lineage by incubation with 2% DMSO for 3 days as previously described (Brand et al., 2004).

TAL1 knockdown in ECFCs

The KD of TAL1 was performed by lentivirus-mediated shRNA. Preparation of lentiviruses expressing 2 different anti-TAL1 shRNA or a scrambled shRNA (negative control), and lentiviral infection were performed as previously described (Palii et al., 2011a; Palii et al., 2011b) with the following modifications that pertain to ECFCs. Lentiviral suspensions were added to 70% confluent ECFCs at a multiplicity of infection (MOI) of 100 in the presence of 4 μ g/ml hexadimethrine bromide (Polybrene, Sigma). ECFCs were infected twice at 24 h interval. The western blot and RTqPCR showing TAL1 KD were performed 48h after the first lentiviral infection (i.e. time 0). All phenotypic assays were started at time 0.

Cell proliferation, cell death and cell surface markers

Cell proliferation was analyzed by measuring 5-ethynyl-2'-deoxyuridine (EdU) incorporation using the Click-iT EdU Alexa Fluor 647 assay (Invitrogen) according to the manufacturer's instructions. Apoptosis was measured by Annexin V staining using the PE Apoptosis Detection Kit I (BD-Pharmingen) according to the manufacturer's instructions. 7-Aminoactinomycin D (7-AAD) was used to exclude necrotic cells. Cell surface markers were measured by labeling cells for 20 min. at 4°C with fluorescein isothiocyanate (FITC), phycoerythrin (PE) or allophycocyanin (APC) -conjugated Abs (see below for a list of Abs). After washing, cells were resuspended in PBS containing 1% BSA and analyzed by flow cytometry. For all experiments, 10,000 cells per sample were recorded on a

BD LSR or a BD LSRFortessa cell analyzer (Becton Dickinson). Flow cytometry controls were unstained cells. Results were analyzed using CELL Quest and Summit v4.3 (for BD LSR) or BD FACSDiva (for BD LSRFortessa).

Immunohistochemistry

At indicated times after ligation surgery, hindlimb muscle tissue was taken distal to the ligation site and frozen in OCT. Muscles were sectioned using a Cryostat (Leica CM 1850). Sections of 12 μm were fixed with 100% cold (-20°C) acetone for 10 min, and stained with the following antibodies: anti- α -smooth muscle actin (α -SMA) (Abcam Cat# 5694), anti- von Willebrand factor (vWF) (Dako Cat#A0082), anti- mouse CD31 (BD Pharmingen Cat#550274), or with an anti-human mitochondria antibody (Millipore Cat# MAB1273) pre-labeled with Alexa Fluor 488 fluorescent mouse IgG1 Zenon probes (Cat#Z25002, Invitrogen) following the manufacturer's instructions. Samples were then processed as described (Lu and Partridge, 1998). Imaging was performed with a Zeiss Z1 fluorescent microscope or with a Zeiss LSM 510 Meta confocal fluorescent microscope as indicated. To quantify vascular density, the number of α -SMA⁺ arterioles per field of view was counted in 3 random microscopic fields (0.5mm^2) per sample in a blinded fashion.

Detection of Human Gene Expression in Murine Ischemic Muscles

Ischemic muscles were dissected, snap frozen in liquid nitrogen and ground in a Bullet Blender (Next Advance Inc. USA) with 0.5mm zirconium silicate beads.

Tissue homogenization was performed in the RLT Plus buffer using a Kontes Pellet Pestle Cordless Motor, followed by DNA and RNA extraction using the AllPrep DNA/RNA Mini Kit protocol (Qiagen, Cat# 80204). Engrafted human cells were detected by measuring human Alu repeats by TaqMan real-time qPCR as previously described (Lee et al., 2006). Expression of specific genes was measured by RTqPCR. Primer and probe sequences are provided below.

Matrigel Assay

Matrigel assays were performed essentially as previously described (Ingram et al., 2004). Briefly, ECFCs in complete EGM-2 medium were seeded onto 48 or 96-well tissue culture plates previously coated with Matrigel (Cat# 356234; BD Biosciences) at a cell density of 20,000 cells or 10,000 cells per well, respectively. Morphogenesis was allowed to proceed for 24h at 37°C. Photographs were taken at 2.5x and 10x magnification using an Axiovert S100 inverted-phase microscope coupled to a Zeiss Axio Camera. For quantification of the network, cells were stained with 5 µg/ml calcein (Cat# 354216, BD Biosciences) for 30 min at 37°C, followed by automatic quantification using the AngioQuant software (Niemisto et al., 2005). Each experiment was carried out in triplicate and repeated at least three times with biologically independent ECFCs.

Collagen Assay

Collagen assays were performed essentially as previously described (Cabrita et al., 2011). Briefly, tissue culture plates were coated with purified bovine collagen (PureCol Cat# 5005-B, Advanced BioMatrix) according to the manufacturer's instructions. ECFCs in complete EGM-2 medium were seeded onto Collagen-coated 12-well plates at a cell density of 80,000 cells per well and incubated for 48h at 37⁰C. Photographs were taken at 2.5x and 10x magnification using an Axiovert S100 inverted-phase microscope coupled to a Zeiss Axio Camera. Each experiment was carried out in triplicate and repeated at least three times with biologically independent ECFCs.

Cell Migration Assay by Gap Closure

ECFCs were resuspended into complete EGM-2 medium and plated onto a radius 24-well cell migration tissue culture plate that contains a centrally located hydrogel plug (Cat# CBA-125; Cell Biolabs) at a density of 0.1 million cells per well. Cells were left to adhere to the plate overnight at 37⁰C and the plug was removed creating a cell-free zone or gap. Cells migrating into the central gap were then counted at indicated time-points under 10x magnification using an Axiovert S100 inverted-phase microscope. At the last time-point, cells were stained with crystal violet. Each experiment was carried out in triplicate and repeated at least three times with biologically independent ECFCs.

Cell Migration Assay by Chemotaxis

Migration of ECFCs by chemotaxis towards SDF-1 α was tested using a 24-well Boyden chamber (8 μ m pore diameter filter; Greiner Bio-One Cat#662638). ECFCs were cultured for 12h without serum prior to being added to the top chamber at a density of 40,000 cells/chamber in 200 μ l serum-free EGM-2 medium supplemented with 0.5% BSA. Cells were allowed to migrate towards the lower chamber containing 100 ng/ml SDF-1 α for 4h. Cells on the filter were fixed in 4% PFA and stained with Diff Quik Stain kit (Fisher Scientific Cat# NC9943455). The upper surface of the membrane was wiped with cotton swabs to remove cells that did not migrate. Cells that had migrated onto the lower surface of the filter were counted at 20x magnification under an Axiovert S100 inverted-phase microscope. Each experiment was carried out in triplicate and repeated at least three times with biologically independent ECFCs.

Adhesion Assay

ECFCs were harvested and resuspended in serum-free EGM-2 medium supplemented with 0.5% BSA. The cells were seeded at 50,000 cells/well onto 6-well plates (CellBIND, Corning) and incubated at 37°C for 30 minutes. The wells were washed three times with PBS to remove unattached cells. Cells that remained attached were stained with DAPI and counted at 10x magnification under a Zeiss Observer.Z1 inverted fluorescence microscope coupled to an

AxioCam HRm. Each experiment was carried out in triplicate and repeated at least three times with biologically independent ECFCs.

Knockdown of CDH5 (VE-cadherin) by siRNA in ECFCs

ECFCs were seeded at a density of 25,000 cells per cm² in EGM-2 medium without antibiotics for 24h. CDH5 knockdown was induced by transfection of anti-CDH5 siRNA (5'-CCAUGAAGCCUCUGGAUUA UU-3' and 3'-UUGGUACUUCGGAGACCUAUU-5') with Lipofectamine 2000 according to the instructions of the manufacturer. A Cy3-labeled control siRNA (Cat# AM4621, Ambion) was used as a negative control. Twenty-four hours after transfection, ECFCs were treated with TSA, and harvested for RNA extraction, immunocytochemistry, Western blotting, cell migration by gap closure assay and hindlimb ischemia assay.

Knockdown of EP300 (p300) by siRNA in ECFCs

ECFCs were seeded at a density of 25,000 cells per cm² in EGM-2 medium without antibiotics for 24h. P300 knockdown was induced by transfection of anti-EP300 siRNA (sc-29431, Santa Cruz) with Lipofectamine 2000 according to the instructions of the manufacturer. A Cy3-labeled control siRNA (Cat# AM4621, Ambion) was used as a negative control. Twenty-four hours after transfection, ECFCs were harvested for RNA extraction, cell migration by gap closure assay and matrigel assay.

Immunocytochemistry

ECFCs in complete EGM-2 medium were seeded on 24-well plates containing 12 mm diameter coverslips at a density of 50,000 cells per well. ECFCs were fixed for 10 min with 4% PFA and stained with anti- TAL-1 and VE-cadherin Abs (see below for information on the antibodies). Imaging was performed with a Zeiss Z1 fluorescent microscope.

Gene Expression Profiling on Affymetrix microarray

Total RNA from 3 independent ECFC colonies (derived from 3 distinct cord blood donors), each with or without a TAL1 KD was isolated using the RNeasy Mini Kit (Qiagen) including a step of on-column DNase I digestion. Labeling and hybridization to the Affymetrix Human Gene 1.0 ST gene expression microarray was performed at the StemCore Laboratories Facility (Ottawa, ON, Canada) following standard Affymetrix procedures. For microarray data analysis, intensity values were normalized with RMA (Gautier et al., 2004). Probesets with low variation were discarded by filtering out those with standard deviations below the first quartile of the deviations global distribution. To detect significant differences in expression between TAL1 KD and control we used Limma (Smyth et al., 2005). A total of 505 probesets (Table S1) showed significant differences (Benjamini-Hochberg adjusted p -value ≤ 0.05). Microarray raw data are deposited into GEO (GSE44444).

Chromatin immunoprecipitation (ChIP)

Enrichment of acetylated histone H3 was measured using a native ChIP protocol (Brand et al., 2008). Binding of transcription factors was measured using a crosslink ChIP protocol as previously described (Palii et al., 2011b). For high-throughput sequencing, ChIPed DNA was amplified using the Illumina protocol with modifications described in (Palii et al., 2011b), and single-end sequencing was performed at the McGill University and Génome Québec Innovation Centre (Montréal, QC) on a Illumina HiSeq 2000. For qPCR, DNA was quantified using SYBROgreen. ChIPed DNA was quantified using a standard curve generated with genomic DNA and was normalized by dividing the amount of the corresponding target in the input fraction.

High-throughput DNA sequencing data analysis to identify TAL1 genomic binding in ECFCs

Reads of 50bp were mapped to the NCBI build 37.1 (h19) human reference genome using MAQ (Li et al., 2008) version 0.7.1 allowing for a maximum of two mismatches. Unmapped reads were truncated to 31 bp and remapped to the genome. Truncation and remapping were repeated down to 26 bp read size. All reads that uniquely mapped to the reference genome were used to identify TAL1 binding sites. To detect regions of enrichment, we used model-based analysis of ChIP combined with massively parallel sequencing (MACS) software (Zhang et

al., 2008) version 1.3.7.1 using a minimum cutoff of 8 tags per enriched region and a p -value threshold for peak significance $< 1 \times 10^{-5}$. ChIP-seq data are deposited in GEO (GSE44442).

High-throughput DNA sequencing data analysis to compare TAL1 genomic binding in TSA-treated versus non-treated ECFCs

TAL1 ChIP-seq experiments were performed in TSA-treated and non-treated ECFCs (data deposited in GEO (GSE53423)). For each data set, reads of 50bp were mapped to the NCBI build 37.1 (h19) human reference genome using BWA (Li and Durbin, 2009) version 0.6.1 allowing for a maximum of two mismatches. Regions of enrichment were detected using MACS (Zhang et al., 2008) version 1.3.7.1 with a low stringency threshold (p -value $\leq 1 \times 10^{-3}$). Binding similarity was estimated by calculating a Pearson Correlation Coefficient (PCC) of read counts under peaks found in either data set.

De novo Motif Discovery

DNA motifs that are overrepresented under peaks of TAL1 binding were identified using the MotifRG Bioconductor package for discriminative motif discovery as previously described (Fong et al., 2012; Palii et al., 2011b) except that shuffled peak sequences generated by uShuffle (Jiang et al., 2008) were used as background.

Detection of Composite DNA motifs

We explored whether there are preferred distances between E-boxes and other identified DNA motifs under peaks of TAL1 binding. As a background we used the regions in Chromosome 1 (hg19 build), masked by RepeatMasker. Composite motifs are shown in Figures 4B and S4B.

Nuclear Extraction and Immunoprecipitation

Nuclear extraction and immunoprecipitation (IP) were performed as previously described (Palii et al., 2011b) except that we used a high stringency wash buffer (25mM Tris-HCl pH 7.9, 5mM MgCl₂, 10% (v/v) Glycerol, 0.1% (v/v) NP-40, 1M KCl, 0.3mM DTT, and protease inhibitors). Elution was performed by heating at 95^oC for 5 min. in SDS-PAGE loading buffer.

Antibodies (Abs)

The following Abs were used for the applications specified below. For FACS: anti- CD31-FITC (Cat# 555445), CD34-FITC (Cat# 555821), CD14-FITC (Cat# 555397), CD105-APC (Cat# 562408), CD144 (Cat# 555661) from BD-Pharmingen, VEGFR2/KDR-APC (Cat# FAB357A) from RD Systems, vWF (Cat# sc-14014) from Santa Cruz Biotechnology and CD45-FITC (Cat# 11-0459-42) from eBioscience. For western blot: anti- TAL1 (Cat# 04-123) from Millipore, TF_{II}Hp89 (Cat# sc-293) from Santa Cruz Biotechnology, acetylated K (Cat# ab193) from Abcam, VE-cadherin (Cat# 555661) from BD Pharmingen and

tubulin (monoclonal Ab from the Developmental Studies Hybridoma Bank developed under the auspices of the NICHD and maintained by The University of Iowa). For immunofluorescence: anti- α -SMA (Cat# 5694) from Abcam, anti- vWF (Cat#A0082) from Dako, anti- mouse CD31 (Cat#550274) and VE-cadherin (Cat# 555661) from BD Pharmingen, and anti- human mitochondria clone 113-1 (Cat# MAB1273) and TAL-1 (Cat# 04-123) from Millipore. For ChIP: anti- TAL1 (Cat# sc-12984), p300 (Cat# sc-585), normal goat IgG (Cat# sc-2028), normal rabbit IgG (Cat# sc-2027) from Santa Cruz Biotechnology and acetylated histone H3 (Cat# 06-599) from Millipore. For IP: anti- TAL1 (Cat# sc-12984) and normal goat IgG (Cat# sc-2028) from Santa Cruz Biotechnology.

RT-qPCR primers

TAL1 RT For: ACCAAAGTTGTGCGGCGTAT
TAL1 RT Rev: AGGCCCGTTCACATTCTG

GAPDH RT For: TCCCTGAGCTGAACGGGAAG
GAPDH RT Rev: GGAGGAGTGGGTGTCTGCTGT

EPHB4 RT For: CAAGCCCCTGTCAGGAGAAG
EPHB4 RT Rev: CAGACGGCTGATCCAATGG

CDH5 RT For: GCGACTACCAGGACGCTTTC
CDH5 RT Rev: GGCTTCATGGGCTTGATGAT

EFNB2 RT For: CCTCTCCTCAACTGTGCCAAA
EFNB2 RT Rev: CCCAGAGGTTAGGGCTGAATT

SOX7 RT For: TCAGCAAGATGCTGGGAAAGT
SOX7 RT Rev: TCCGCCTCGTCCACGTA

HOXA9 RT For: AGCCGGCCTTATGGCATTAA

HOXA9 RT Rev: CAGGGACAAAGTGTGAGTGTCAA

CNN2 RT For: CAACTTCATCAAGGCCATGGT
CNN2 RT Rev: TCCCACTCTCAAACAGGTCGTT

CD93 RT For: GAGGATGAGCAAGTTCTGGATTG
CD93 RT Rev: CGCCCACCCAGCTGAA

ELP3 RT For: TTGGCCTCCTACGATTACGCAAGT
ELP3 RT Rev: ACACTCCCATACACATGCAGCTCT

EP300 RT For: GATGACCCTTCCCAGCCTCAAA
EP300 RT Rev: GCCAGATGATTCATGGTGAAGG

CXCR4 RT For: TGGCATTGTGGGCAATGGATTGGT
CXCR4 RT Rev: TACCAGTTTGCCACGGCATCAACT

VEGFA RT For: TGG TCC CAG GCT GCA CCC AT
VEGFA RT Rev: CGC ATC GCA TCA GGG GCA CA

Rodent GAPDH primers (Applied Biosystems Cat# 4308313)

qPCR primers

CDH5 ChIP For: TCGTTTATGTCAAAGCCTTGTGA
CDH5 ChIP Rev: GTGTCATCCTGGAGCCACAGT

EFNB2 ChIP For: CCATTTCCAAACGTGGTAATCA
EFNB2 ChIP Rev: AATTGTTCTTGAAGCAGGAAATCTG

SOX7 ChIP For: TCACTCACCCAGCATCTTGCT
SOX7 ChIP Rev: CATGGTTTGGGCCAAGGA

HOXA9 ChIP For: GCCTGCCCTATCCTTCCTAGTC
HOXA9 ChIP Rev: CACCAGTCCCGGGTGTGA

ADAM19 ChIP For: AAAGGTCAGAAGGAGAGGTTGATG
ADAM19 ChIP Rev: GGTGGAAGTGGGCATGATTC

CNN2 ChIP For: CCCTGGTTTATATACGAGGAACTGA
CNN2 ChIP Rev: AACCCCAGGAGCTGCTCTTC

CD93 ChIP For: AGCCATCCCCCCTTCA
CD93 ChIP Rev: CCCCAAGTATGGCTGCAACTT

RUNX1T1 ChIP For: CGTGCATCAGGGTGATTACAA
RUNX1T1 ChIP Rev: TCCCGCTCCGTCTACA

ZNF175 ChIP For: AACTTCCAGTTCTAAACCACACTCAA
ZNF175 ChIP Rev: GAGTCACTGTGCCTGTCTAAGTTCTT

PCDH7 ChIP For: GAACGAGTGCTTCCTGGACTTC
PCDH7 ChIP Rev: CGATGACCTGACCCTCAAACA

FAM69B ChIP For: CCACCCCCCATTGTTTCTCT
FAM69B ChIP Rev: GCCCCCTCAGACCACTTGT

NRARP ChIP For: GCCGATTCTGAACAGCTCATT
NRARP ChIP Rev: GTCCGCTGCCTCTCTTTGTC

ANGPTL4 ChIP For: TGTTTCCCGTCCCTTCACA
ANGPTL4 ChIP Rev: CAAGTGATGAACGGCATTGG

ELP3 ChIP For: CCCAGGTCGAGCTTTCTAACC
ELP3 ChIP Rev: GGGTCTCAGGGATGGAGGAT

ANGPTL2 ChIP For: GAGTCCAAGGCTGTCCACACA
ANGPTL2 ChIP Rev: CTAAGCCACTGCCTCCTGCTA

ETS1 ChIP For: CCCACAGGATGGACCCTTT
ETS1 ChIP Rev: AGAGCCCCCTGAGCTGAATC

Alu For: CATGGTGAAACCCCGTCTCTA
Alu Rev: GCCTCAGCCTCCCGAGTAG
Alu Probe: FAM-ATTAGCCGGGCGTGGTGGCG-BHQ1

Supplemental References

- Brand, M., Rampalli, S., Chaturvedi, C.P., and Dilworth, F.J. (2008). Analysis of epigenetic modifications of chromatin at specific gene loci by native chromatin immunoprecipitation of nucleosomes isolated using hydroxyapatite chromatography. *Nat Protoc* **3**, 398-409.
- Brand, M., Ranish, J.A., Kummer, N.T., Hamilton, J., Igarashi, K., Francastel, C., Chi, T.H., Crabtree, G.R., Aebersold, R., and Groudine, M. (2004). Dynamic changes in transcription factor complexes during erythroid differentiation revealed by quantitative proteomics. *Nat Struct Mol Biol* **11**, 73-80.
- Cabrita, M.A., Jones, L.M., Quizi, J.L., Sabourin, L.A., McKay, B.C., and Addison, C.L. (2011). Focal adhesion kinase inhibitors are potent anti-angiogenic agents. *Mol Oncol* **5**, 517-526.
- Ernst, J., and Kellis, M. (2012). ChromHMM: automating chromatin-state discovery and characterization. *Nat Methods* **9**, 215-216.
- Fong, A.P., Yao, Z., Zhong, J.W., Cao, Y., Ruzzo, W.L., Gentleman, R.C., and Tapscott, S.J. (2012). Genetic and epigenetic determinants of neurogenesis and myogenesis. *Dev Cell* **22**, 721-735.
- Gautier, L., Cope, L., Bolstad, B.M., and Irizarry, R.A. (2004). affy--analysis of Affymetrix GeneChip data at the probe level. *Bioinformatics* **20**, 307-315.
- Ingram, D.A., Mead, L.E., Tanaka, H., Meade, V., Fenoglio, A., Mortell, K., Pollok, K., Ferkowicz, M.J., Gilley, D., and Yoder, M.C. (2004). Identification of a novel hierarchy of endothelial progenitor cells using human peripheral and umbilical cord blood. *Blood* **104**, 2752-2760.
- Jiang, M., Anderson, J., Gillespie, J., and Mayne, M. (2008). uShuffle: a useful tool for shuffling biological sequences while preserving the k-let counts. *BMC Bioinformatics* **9**, 192.
- Lee, R.H., Hsu, S.C., Munoz, J., Jung, J.S., Lee, N.R., Pochampally, R., and Prockop, D.J. (2006). A subset of human rapidly self-renewing marrow stromal cells preferentially engraft in mice. *Blood* **107**, 2153-2161.
- Li, H., and Durbin, R. (2009). Fast and accurate short read alignment with Burrows-Wheeler transform. *Bioinformatics* **25**, 1754-1760.
- Li, H., Ruan, J., and Durbin, R. (2008). Mapping short DNA sequencing reads and calling variants using mapping quality scores. *Genome Res* **18**, 1851-1858.
- Lu, Q.L., and Partridge, T.A. (1998). A new blocking method for application of murine monoclonal antibody to mouse tissue sections. *The journal of histochemistry and cytochemistry : official journal of the Histochemistry Society* **46**, 977-984.
- McLean, C.Y., Bristor, D., Hiller, M., Clarke, S.L., Schaar, B.T., Lowe, C.B., Wenger, A.M., and Bejerano, G. (2010). GREAT improves functional interpretation of cis-regulatory regions. *Nat Biotechnol* **28**, 495-501.

Niemisto, A., Dunmire, V., Yli-Harja, O., Zhang, W., and Shmulevich, I. (2005). Robust quantification of in vitro angiogenesis through image analysis. *IEEE transactions on medical imaging* 24, 549-553.

Palii, C.G., Pasha, R., and Brand, M. (2011a). Lentiviral-mediated knockdown during ex vivo erythropoiesis of human hematopoietic stem cells. *J Vis Exp*.

Palii, C.G., Perez-Iratxeta, C., Yao, Z., Cao, Y., Dai, F., Davison, J., Atkins, H., Allan, D., Dilworth, F.J., Gentleman, R., *et al.* (2011b). Differential genomic targeting of the transcription factor TAL1 in alternate haematopoietic lineages. *EMBO J* 30, 494-509.

Parks, D.H., and Beiko, R.G. (2010). Identifying biologically relevant differences between metagenomic communities. *Bioinformatics* 26, 715-721.

Sanda, T., Lawton, L.N., Barrasa, M.I., Fan, Z.P., Kohlhammer, H., Gutierrez, A., Ma, W., Tatarek, J., Ahn, Y., Kelliher, M.A., *et al.* (2012). Core transcriptional regulatory circuit controlled by the TAL1 complex in human T cell acute lymphoblastic leukemia. *Cancer Cell* 22, 209-221.

Smyth, G.K., Michaud, J., and Scott, H.S. (2005). Use of within-array replicate spots for assessing differential expression in microarray experiments. *Bioinformatics* 21, 2067-2075.

Yoder, M.C., Mead, L.E., Prater, D., Krier, T.R., Mroueh, K.N., Li, F., Krasich, R., Temm, C.J., Prchal, J.T., and Ingram, D.A. (2007). Redefining endothelial progenitor cells via clonal analysis and hematopoietic stem/progenitor cell principals. *Blood* 109, 1801-1809.

Zhang, Y., Liu, T., Meyer, C.A., Eeckhoutte, J., Johnson, D.S., Bernstein, B.E., Nusbaum, C., Myers, R.M., Brown, M., Li, W., *et al.* (2008). Model-based analysis of ChIP-Seq (MACS). *Genome Biol* 9, R137.